
Multi-Agent Reinforcement Learning for Active Voltage Control on Power Distribution Networks

Jianhong Wang*

Imperial College London
jianhong.wang16@imperial.ac.uk

Wangkun Xu*

Imperial College London
wangkun.xu18@imperial.ac.uk

Yunjie Gu[†]

University of Bath
yg934@bath.ac.uk

Wenbin Song

ShanghaiTech University
songwb@shanghaitech.edu.cn

Tim C. Green[‡]

Imperial College London
t.green@imperial.ac.uk

Abstract

This paper presents a problem in power networks that creates an exciting and yet challenging real-world scenario for application of multi-agent reinforcement learning (MARL). The emerging trend of decarbonisation is placing excessive stress on power distribution networks. Active voltage control is seen as a promising solution to relieve power congestion and improve voltage quality without extra hardware investment, taking advantage of the controllable apparatuses in the network, such as roof-top photovoltaics (PVs) and static var compensators (SVCs). These controllable apparatuses appear in a vast number and are distributed in a wide geographic area, making MARL a natural candidate. This paper formulates the active voltage control problem in the framework of Dec-POMDP and establishes an open-source environment. It aims to bridge the gap between the power community and the MARL community and be a drive force towards real-world applications of MARL algorithms. Finally, we analyse the special characteristics of the active voltage control problems that cause challenges (e.g. interpretability) for state-of-the-art MARL approaches, and summarise the potential directions.

1 Introduction

Multi-agent reinforcement learning (MARL) has demonstrated impressive performances on games (e.g., Chess [1], StarCraft [2, 3], and etc.) and robotics [4]. There are now increasing interests and thrusts to apply MARL in real-world problems. Power network is a natural test field for MARL algorithms. There are many problems in power networks involving the collaborative or competitive actions of a vast number of agents, such as market bidding [5], voltage control, frequency control, and emergency handling [6]. One of the obstacles for applying MARL in power networks is the lack of transparency and guarantee, which is unacceptable considering the importance of reliable power supply for the whole society. Therefore, it is sensible to start with problems that are less sensitive to reliability but hard to be solved by conventional methods.

Active voltage control in power distribution networks is such a candidate problem. The voltage control problem has been studied for years but only comes under spot light recently due to the increasing penetration of distributed resources, e.g. roof-top photovoltaics (PVs) [7]. The excessive active power injection may cause voltage fluctuations beyond the threshold of grid standards [8]. The voltage fluctuations can be relieved by exploiting the control flexibility of PV inverters themselves

*Equal contributions. [†] Correspondence to Yunjie Gu who is also an honorary lecturer at Imperial College London. [‡] Tim C. Green is also the co-director of the Energy Futures Laboratory (EFL).

along with other controllable apparatuses, such as static var compensators (SVCs) and on load tap changers (OLTCs). An elaborate scheme is needed to coordinate these multiple apparatuses at scale to regulate voltage throughout the network with limited local information, which is called active voltage control [9–12]. The active voltage control problem has many interesting properties. (1) It is a combination of local and global problem, i.e., the voltage of each node is influenced by the powers (real and reactive) of all other nodes but the impact recedes with increasing distance between nodes. (2) It is a constrained optimisation problem where the constraint is the voltage threshold and the objective is the total power loss, but there is no explicit relationship between the constraint and the control action. (3) A distribution network has a radial topology involving a rich structure that can be taken as prior knowledge for control, but the node-branch parameters of the topology may be significantly uncertain. (4) Voltage control has a relatively large tolerance and less severe consequences if the control fails to meet standard requirements.

There have been several attempts to apply MARL in active voltage control [6, 13–16]. Each work on a particular case showed promising performances of state-of-the-art MARL approaches with modifications adapting to the active voltage control problem. However, it is not clear if these methods scale well to a larger network, and the robustness against different scenarios, such as penetration levels and load profiles, are yet to be investigated. There is no commonly accepted benchmark to provide the basis for fair comparison of different solutions.

To facilitate further research on this topic, and to bridge the gap between the power community and MARL community, we present a comprehensive test-bench and open-source environment for MARL based active voltage control. We formally define the active voltage control problem as a Dec-POMDP [17] that is widely acknowledged in the MARL community. We present an environment in Python and construct 3 scenarios with real public data that span from small scale (i.e. 6 agents) to large scale (i.e. 38 agents).

The contributions of this paper are summarised as follows: (1) We formally define the active voltage control problem as a Dec-POMDP and develop an open-source environment.² (2) We conduct large scale experimentation with 7 state-of-the-art MARL algorithms on different scenarios of the active voltage control problem. (3) We convert voltage constraints to barrier functions and observe the importance of designing an appropriate voltage barrier function from the experimental results. (4) By analysing the experimental results, we imply the possible challenges (e.g. interpretability) for MARL to solve the active voltage control problem and suggest potential directions for future works.

2 Related Work

Traditional Methods for Active Voltage Control. Voltage rising and fluctuation problem in distribution networks has been studied for 20 years [18]. The traditional voltage regulation devices such as OLTC and capacitor banks [10] are often installed at substations and therefore may not be effective in regulating voltages at the far end of the line [19]. The emergence of distributed generation, such as roof-top PVs, introduces new approaches for voltage regulation by the active reactive power control of grid-connected inverters [11]. The state-of-the-art active voltage control strategies can be roughly classified into two categories: (1) reactive power dispatch based on optimal power flow (OPF) [20, 21]; and (2) droop control based on local voltage and power measurements [22, 23]. Specifically, centralised OPF [24–26] minimises the power loss while fulfilling voltage constraints (e.g. power flow equation defined in Eq.1); distributed OPF [27, 28] used distributed optimization techniques, such as alternating direction method of multipliers (ADMM), to replace the centralised solver. The primary limitation of OPF is the need of exact system model [29]. Besides, solving constrained optimisation problem is time-consuming, so it is difficult to react to the rapid change of load profile [30]. On the other hand, droop control only depends on its local measurements, but its performance relies on the manually-designed parameters and is often sub-optimal due to the lack of global information [30]. It is possible to enhance droop control by distributed algorithms, but extra communications are needed [31, 19]. In this paper we investigate the possibility of applying MARL techniques on the active voltage control problem. Compared with the previous works on traditional methods, (1) MARL is model-free, so no exact system model is needed; and (2) the response of MARL is fast so as to handle rapid changes of environments (e.g. the intermittency of renewable energy).

²<https://github.com/Future-Power-Networks/MAPDN>.

Multi-Agent Reinforcement Learning for Active Voltage Control. In this section, we discuss the works that applied MARL to active voltage control problem in the power system community. [14, 16] applied MADDPG with the reactive power of inverters or static var compensators (SVCs) as control actions. [32] applied MADDPG with a manually designed voltage inner loop, so that agents set reference voltage instead of reactive power as their control actions. [13] applied MATD3 also with reactive power as control actions. [15] applied MASAC, where both reactive power and the curtailment of active power are used as control actions. In the above works, distribution networks are divided into regions, with each region controlled by a single agent [33]. It is not clear if these MARL approaches scales well for increasing number of agents. In particular, it is not clear if each single inverter in a distribution network can behave as an independent agent. In this work, we model the active voltage control problem as a Dec-POMDP [17], where each inverter is controlled by an agent. We propose Bowl-shape as a barrier function to represent voltage constraint as part of the reward. We build up an open-source environment for this specific problem that can be easily deployed with the existing MARL algorithms.

Concurrent Works. L2RPN [34] is an environment mainly for the centralised control over power transmission networks with node-splitting and lines switch-off for topology management. Gym-ANM [35] is an environment for centralised power distribution network management. Compared with these 2 works, our environment mainly focuses on solving the active voltage control problem in power distribution networks, with the decentralised/distributed manner. Moreover, we provide more complicated scenarios with the real-world data. Finally, our environment can be easily and flexibly extended with more network topologies and data, thanks to the supports of PandaPower [36] and SimBench [37].

3 Background

3.1 Power Distribution Network

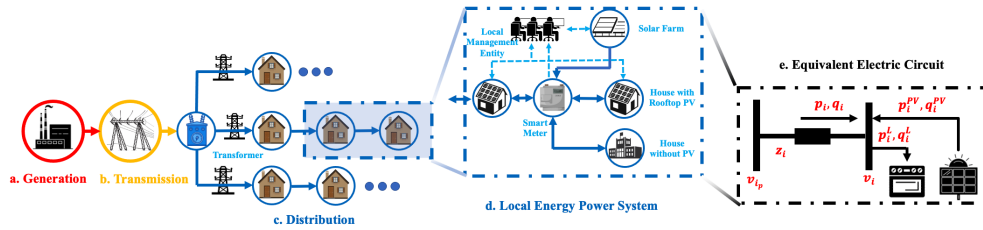


Figure 1: Illustration on distribution network (block a-b-c) under PV penetration. The solid and dotted lines represent the power and information flows respectively. Block d is the detailed version of distribution network and block e is the circuit model of block d.

An electric power distribution network is illustrated in Figure 1 stage a to c. The electricity is generated from power plant and transmitted through transmission lines. Multi-stage transformers are applied to reduce the voltage levels while the electricity is being delivered to the distribution network. The electricity is then consumed by residential and industrial clients. A typical PV unit consists of PV panels and voltage-source inverters which can be installed either on roof-top or in the solar farm. Conventionally, there exist management entities such as distributed system operator (DSO) monitoring and operating the PV resources through the local communication channels. With emergent PV penetration, distribution network gradually grows to be an active participant in power networks that can deliver power and service to its users and the main grid (see the bidirectional power flows in Figure 1 stage-d).

System Model and Voltage Deviation. In this paper, we consider medium (10-24kV) and low (0.23-1kV) voltage distribution networks where PVs are highly penetrated. We model the distribution network in Figure 1 as a tree graph $\mathcal{G} = (V, E)$, where $V = \{0, 1, \dots, N\}$ and $E = \{1, 2, \dots, N\}$ represent the set of nodes (buses) and edges (branches) respectively [24]. Bus 0 is considered as the connection to the main grid, balancing the active and reactive power in the distribution network. For each bus $i \in V$, let v_i and θ_i be the magnitude and phase angle of the complex voltage and $s_j = p_i + jq_i$ be the complex power injection. Then the active and reactive power injection can be

defined as follows:

$$\begin{aligned} p_i^{PV} - p_i^L &= v_i^2 \sum_{j \in V_i} g_{ij} - v_i \sum_{j \in V_i} v_j (g_{ij} \cos \theta_{ij} + b_{ij} \sin \theta_{ij}), \quad \forall i \in V \setminus \{0\} \\ q_i^{PV} - q_i^L &= -v_i^2 \sum_{j \in V_i} b_{ij} + v_i \sum_{j \in V_i} v_j (g_{ij} \sin \theta_{ij} + b_{ij} \cos \theta_{ij}), \quad \forall i \in V \setminus \{0\} \end{aligned} \quad (1)$$

where $V_i := \{j \mid (i, j) \in E\}$ is the index set of buses connected to bus i . g_{ij} and b_{ij} are the conductance and susceptance on branch (i, j) . $\theta_{ij} = \theta_i - \theta_j$ is the phase difference between bus i and j . p_i^{PV} and q_i^{PV} are the active power and reactive power of the PV on the bus i (that are zeros if there is no PV on the bus i). p_i^L and q_i^L are the active power and reactive power of the loads on the bus i (that are zeros if there is no loads on the bus i). Eq.1 can represent the power system dynamics which is essential for solving the power flow problem and active voltage control problem [38] (details in Appendix A.1-A.2). For safe and optimal operation, 5% voltage deviation is usually allowed, i.e., $v_0 = 1.0$ per unit (*p.u.*) and $0.95 \text{ p.u.} \leq v_i \leq 1.05 \text{ p.u.}, \forall i \in V \setminus \{0\}$. When the load is heavy during the nighttime, the end-user voltage could be smaller than 0.95 p.u. [39]. In contrast, to export its power, large penetration of p_i^{PV} leads to reverse current flow that would increase v_i out of the nominal range (Figure 1-d) [18, 40].

Optimal Power Flow. In this paper, OPF is regarded as an optimization problem minimizing the total power loss subject to the power balance constraints defined in Eq.1, PV reactive power limits, and bus voltage limits [41]. As the centralized OPF has full access to the system topology, measurements, and PV resources, it provides the optimal active voltage control performance and can be used as a benchmark method (details in Appendix A.3). However, the performance of the OPF depends on the accuracy of the grid model and the optimisation is time-consuming which makes it difficult to be deployed online.

Droop Control. To regulate local voltage deviation, the standard droop control defines a piece-wise linear relationship between PV reactive power generation and voltage deviation at a bus equipped with inverter-based PVs [30, 42] (details in Appendix A.4). It is a fully decentralised control and ignore both the total voltage divisions and the power loss.

3.2 Dec-POMDP

Multi-agent reinforcement learning (MARL) is an extension from the reinforcement learning problem, with multiple agents in the same environment. The problem of MARL for cooperation among agents is conventionally formulated as a Dec-POMDP [17]. It is usually formulated as a tuple such that $\langle \mathcal{I}, \mathcal{S}, \mathcal{A}, \mathcal{O}, \mathcal{T}, r, \Omega, \rho, \gamma \rangle$. \mathcal{I} is an agent set; \mathcal{S} is a state set; $\mathcal{A} = \times_{i \in \mathcal{I}} \mathcal{A}_i$ is the joint action set, where \mathcal{A}_i is each agent's action set; $\mathcal{O} = \times_{i \in \mathcal{I}} \mathcal{O}_i$ is the joint observation set, where \mathcal{O}_i is each agent's observation set; $\mathcal{T} : \mathcal{S} \times \mathcal{A} \times \mathcal{S} \rightarrow [0, 1]$ is a transition probability function that describes the dynamics of an environment; $r : \mathcal{S} \times \mathcal{A} \rightarrow \mathbb{R}$ is a global reward function that describes the award to the whole agents given their decisions; $\Omega : \mathcal{S} \times \mathcal{A} \times \mathcal{O} \rightarrow [0, 1]$ describes the perturbation of the observers (or sensors) for agents' joint observations over the states after decisions; $\rho : \mathcal{S} \rightarrow [0, 1]$ is a probability function of initial states; and $\gamma \in (0, 1)$ is a discount factor. The objective of Dec-POMDP is finding an optimal joint policy $\pi = \times_{i \in \mathcal{I}} \pi_i$ that solves $\max_{\pi} \mathbb{E}_{\pi} \left[\sum_{t=0}^{\infty} \gamma^t r_t \right]$.

4 Distributed Active Voltage Control Problem

4.1 Problem Formulation

For the ease of operations, a large-scale power network is divided into multiple regions and there are several PVs installed into each region that is managed by the responsible distribution network owner. Each PV is with an inverter that generates reactive power to control the voltage around a stationary value denoted as v_{ref} . In our problem, we assume that the PV ownership (e.g. individual homeowners or enterprise) is independent and separated from the distribution network ownership (DNO) [33]. Specifically, a PV owner is responsible for operating a PV infrastructure. In other words, each PV is able to be controlled under a distributed manner so that it is natural to be considered as an agent. To enforce the safety of distribution power networks, all agents (i.e. PVs) within a region share the

observation of this region.³ Since each agent can only observe partial information of the whole grid and maintaining the safety of the power network is a common goal among agents, it is reasonable to model the problem as a Dec-POMDP [17] that can be mathematically described as a 10-tuple such that $\langle \mathcal{I}, \mathcal{S}, \mathcal{A}, \mathcal{R}, \mathcal{O}, \mathcal{T}, r, \Omega, \rho, \gamma \rangle$, where ρ is the probability distribution for drawing the initial state and γ is the discount factor.

Agent Set. There is a set of agents controlling a set of PV inverters denoted as \mathcal{I} . Each agent is located at some node in \mathcal{G} (i.e. a graph representing the power network defined as before). We define a function $g : \mathcal{I} \rightarrow V$ to indicate the node where an agent is located.

Region Set. The whole power network is separated into M regions, whose union is denoted as $\mathcal{R} = \{\mathcal{R}_k \subset V \mid k < M, k \in \mathbb{N}\}$, where $\bigcup_{\mathcal{R}_k \in \mathcal{R}} \mathcal{R}_k \subseteq V$ and $\mathcal{R}_{k_1} \cap \mathcal{R}_{k_2} = \emptyset$ if $k_1 \neq k_2$. We define a function $f : V \rightarrow \mathcal{R}$ that maps a node to the region where it is involved.

State and Observation Set. The state set is defined as $\mathcal{S} = \mathcal{L} \times \mathcal{P} \times \mathcal{Q} \times \mathcal{V}$, where $\mathcal{L} = \{(\mathbf{p}^L, \mathbf{q}^L) : \mathbf{p}^L, \mathbf{q}^L \in (0, \infty)^{|V|}\}$ is a set of (active and reactive) powers of loads; $\mathcal{P} = \{\mathbf{p}^{PV} : \mathbf{p}^{PV} \in (0, \infty)^{|\mathcal{I}|}\}$ is a set of active powers generated by PVs; $\mathcal{Q} = \{\mathbf{q}^{PV} : \mathbf{q}^{PV} \in (0, \infty)^{|\mathcal{I}|}\}$ is a set of reactive powers generated by PV inverters at the preceding step; $\mathcal{V} = \{(\mathbf{v}, \theta) : \mathbf{v} \in (0, \infty)^{|V|}, \theta \in [-\pi, \pi]^{|V|}\}$ is a set of voltage wherein \mathbf{v} is a vector of voltage magnitudes and θ is a vector of voltage phases measured in radius. $v_i, p_i^L, q_i^L, p_i^{PV}$ and q_i^{PV} are denoted as the components of the vectors $\mathbf{v}, \mathbf{p}^L, \mathbf{q}^L, \mathbf{p}^{PV}$ and \mathbf{q}^{PV} respectively. We define a function $h : \mathbb{P}(V) \rightarrow \mathbb{P}(\mathcal{S})$ that maps a subset of V to its correlated measures, where $\mathbb{P}(\cdot)$ denotes the power set. The observation set is defined as $\mathcal{O} = \times_{i \in \mathcal{I}} \mathcal{O}_i$, where $\mathcal{O}_i = (h \circ f \circ g)(i)$ indicates the measures within the region where agent i is located.

Action Set. Each agent $i \in \mathcal{I}$ is equipped with a continuous action set $\mathcal{A}_i = \{a_i : -c \leq a_i \leq c, c > 0\}$. The continuous action represents the ratio of maximum reactive power it generates, i.e., the reactive power generated from the k th PV inverter is $q_k^{PV} = a_k \sqrt{(s_k^{\max})^2 - (p_k^{PV})^2}$, where s_k^{\max} is the maximum apparent power of the k th node that is dependent on the physical capacity of the PV inverter.^{4,5} If $a_k > 0$, it means penetrating reactive powers to the distribution network. If $a_k < 0$, it means absorbing reactive powers from the distribution network. The value of c is usually selected as per the loading capacity of a distribution network, which is for the safety of operations. The joint action set is denoted as $\mathcal{A} = \times_{i \in \mathcal{I}} \mathcal{A}_i$.

State Transition Probability Function. Since the state includes the last action and the change of loads is random (that theoretically can be modelled as any probabilistic distribution), we can naturally define the state transition probability function as $\mathcal{T} : \mathcal{S} \times \mathcal{A} \times \mathcal{S} \rightarrow [0, 1]$ that follows Markov decision process. Specifically, $\mathcal{T}(\mathbf{s}_{t+1} | \mathbf{s}_t, \mathbf{a}_t) = Pr(\mathbf{s}_{t+1} | \delta(\mathbf{s}_t, \mathbf{a}_t))$, where $\mathbf{a}_t \in \mathcal{A}$ and $\mathbf{s}_t, \mathbf{s}_{t+1} \in \mathcal{S}$. $\delta(\mathbf{s}_t, \mathbf{a}) \mapsto \mathbf{s}_{t+\tau}$ denotes the solution of the power flow, whereas $Pr(\mathbf{s}_{t+1} | \mathbf{s}_{t+\tau})$ describes the change of loads (i.e. highly correlated to the user behaviours). $\tau \ll \Delta t$ is an extremely short interval much less than the time interval between two controls (i.e. a time step) and $\Delta t = 1$ in this paper.

Observation Probability Function. We now define the observation probability function. In the context of electric power network, it describes the measurement errors that may occur in sensors. Mathematically, we can define it as $\Omega : \mathcal{S} \times \mathcal{A} \times \mathcal{O} \rightarrow [0, 1]$. Specifically, $\Omega(\mathbf{o}_{t+1} | \mathbf{s}_{t+1}, \mathbf{a}_t) = \mathbf{s}_{t+1} + \mathcal{N}(\mathbf{0}, \Sigma)$, where $\mathcal{N}(\mathbf{0}, \Sigma)$ is an isotropic multi-variable Gaussian distribution and Σ is dependent on the physical properties of sensors (e.g. smart meters).

Reward Function. The reward function is defined as follows:

$$r = -\frac{1}{|V|} \sum_{i \in V} l_v(v_i) - \alpha \cdot l_q(\mathbf{q}^{PV}), \quad (2)$$

where $l_v(\cdot)$ is a voltage barrier function and $l_q(\mathbf{q}^{PV}) = \frac{1}{|\mathcal{I}|} \|\mathbf{q}^{PV}\|_1$ is the reactive power generation loss (i.e. a type of power loss approximation easy for computation). The objective is to control the voltage within a safety range around v_{ref} , while the reactive power generation is as less as possible, i.e.,

³Sharing observation in this problem is reasonable, since only the sensor measurements (e.g. voltage, active power, etc.) are shared, which are not directly related to the commercial profits [33]. The observation of each PV is collected by the distribution network owner and then the full information within the region is sent to each agent.

⁴Note that the reactive power range actually dynamically changes at each time step.

⁵Yielding $(q_k^{PV})_t$ at each time step t is equivalent to yielding $\Delta_t(q_k^{PV})$ (i.e. the change of reactive power generation at each time step), since $(q_k^{PV})_t = (q_k^{PV})_{t-1} + \Delta_t(q_k^{PV})$. For easily satisfying the safety condition, we directly yield q_k^{PV} at each time step in this work.

$l_q(\mathbf{q}^{PV}) < \epsilon$ and $\epsilon > 0$. Similar to the mathematical tricks used in β -VAE [43], by KKT conditions we can transform a constrained reward to a unconstrained reward with a Lagrangian multiplier $\alpha \in (0, 1)$ shown in Eq.2. Since $l_v(\cdot)$ is not easy to define in practice (i.e., it affects $l_q(\mathbf{q}^{PV})$), we aim to study for a good choice in this paper.

Objective Function. The objective function of this problem is $\max_{\pi} \mathbb{E}_{\pi}[\sum_{t=0}^{\infty} \gamma^t r_t]$, where $\pi = \times_{i \in \mathcal{I}} \pi_i$; $\pi_i : \bar{\mathcal{O}}_i \times \mathcal{A}_i \rightarrow [0, 1]$ and $\bar{\mathcal{O}}_i = (\mathcal{O}_i^{\tau})_{\tau=1}^h$ is a history of observations with the length as h . Literally, we need to find an optimal joint policy π to maximize the discounted cumulative rewards.

4.2 Voltage Barrier Function

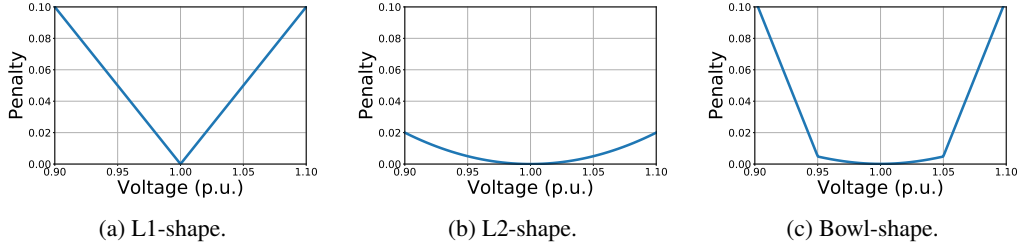


Figure 2: This figure shows 3 voltage barrier functions, where L1-shape and L2-shape are 2 baselines while Bowl-shape is proposed in this paper.

We define $v_{\text{ref}} = 1 \text{ p.u.}$ in this paper, and the voltage needs to be controlled within the safety range from 0.95 p.u. to 1.05 p.u. , which sets the constraint of control. The voltage constraint is difficult to be handled in MARL, so we use a barrier function to represent the constraint. L1-shape (see Figure 2a) was most frequently used in the previous work [13–15], however, this may lead to wasteful reactive power generations since $\frac{|\Delta l_v|}{\alpha |\Delta l_q|} \gg 1$ within the safety range of voltage. Although L2-shape (see Figure 2b) may alleviate this problem, it may be slow to guide the policy outside the safety range. To address these problems, we propose a barrier function called Bowl-shape that combines the advantages of L1-shape and L2-shape. It gives a steep gradient outside the safety range, while it provides a slighter gradient as voltage tends to the v_{ref} that enables $\frac{|\Delta l_v|}{\alpha |\Delta l_q|} \rightarrow 0$ as $v \rightarrow v_{\text{ref}}$.

5 Experiments

5.1 Experimental Settings

Power Network Topology. Two MV networks, IEEE 33-bus [44] and 141-bus [45] are modified as systems under test.⁶ To show the flexibility on network with multi-voltage levels, we construct a 110kV-20kV-0.4kV (high-medium-low voltage) 322-bus network using benchmark topology from SimBench [37]. For each network, a main branch is firstly determined and the control regions are partitioned by the shortest path between the terminal bus and the coupling point on the main branch. Each region consists of 1-4 PVs dependent on various regional sizes. The specific network descriptions and partitions are shown in Appendix D.1. To give a picture of the tasks, we demonstrate the 33-bus network in Figure 3.

Data Descriptions. The load profile of each network is modified based on the real-time Portuguese electricity consumption accounting for 232 consumers of 3 years.⁷ To highlight the differences between residential and industrial users, we randomly perturb $\pm 5\%$ on the default power factors defined in the case files and accordingly generate real-time reactive power consumption. The solar data is collected from Elia group,⁸ i.e. a Belgium’s power network operator. The load and PV data are then interpolated with 3-min resolution that is consistent with the real-time control period in the grid. To distinguish among different solar radiation levels in various regions, the 3-year PV generations

⁶The original topologies and parameters can be found in MATPOWER [46] description file such as <https://github.com/MATPOWER/matpower/tree/master/data>.

⁷<https://archive.ics.uci.edu/ml/datasets/ElectricityLoadDiagrams20112014>.

⁸<https://www.elia.be/en/grid-data/power-generation/solar-pv-power-generation-data>.

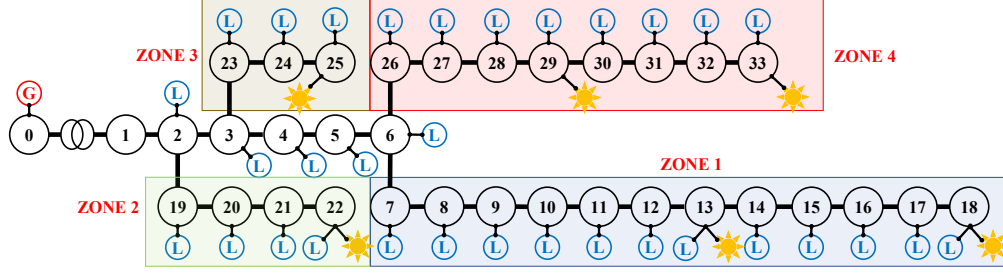


Figure 3: Illustration on 33-bus network. Each bus is indexed by a circle with a number. 4 control regions are partitioned by the smallest path from the terminal to the main branch (bus 1-6). We control the voltages on bus 2-33 whereas bus 0-1 represent the substation or main grid with the constant voltage and infinite active and reactive power capacity. **G** represents an external generator; small **L**s represent loads; and the sun emoji represents the location where a PV is installed.

from 10 cities/regions are collected and PVs in the same control region possess the same generation profiles. We define the PV penetration rate (PR) as the ratio between rated PV generation and rated load consumption. In this paper, we set $PR \in \{2.5, 4, 2.5\}$ as the default PR for different topologies. We oversize each PV inverter by 20% of its maximum active power generation to satisfy the IEEE grid code [42]. Besides, each PV inverter is considered to be able to generate reactive power in the STATCOM mode during night [47]. The median and 25%-75% quantile shadings of PV generations, and the mean and minima-maxima shading of the loads are illustrated in Figure 4. The details can be found in Appendix D.2.

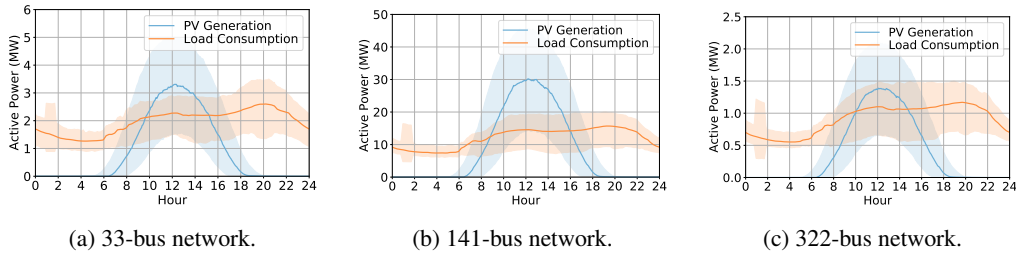


Figure 4: Active PV generations and load consumption.

MARL Simulation Settings. We now describe the simulation settings standing by the view of MARL. In 33-bus network, there are 4 regions with 6 agents. In 141-bus network, there are 9 regions with 22 agents. In 322-bus network, there are 22 regions with 38 agents. The discount factor γ is set to 0.99. α in Eq.2 is set to 0.1. To guarantee the safety of distribution networks, we manually set the range of actions for each scenario, with $[-0.8, 0.8]$ for 33-bus network, $[-0.6, 0.6]$ for 141-bus network, and $[-0.8, 0.8]$ for 322-bus network. During training, we randomly sample the initial state for an episode and each episode lasts for 240 time steps (i.e. a half day). Every experiment is run with 5 random seeds and the test results during training are given by the median and the 25%-75% quartile shading. Each test is conducted every 20 episodes with 10 randomly selected episodes for evaluation.

Evaluation Metrics. In experiments, we use two metrics to evaluate the performance of algorithms.

- *Controllable rate (CR)*: It calculates the ratio of time steps where all buses' voltages being under control during each episode.
- *Power loss (PL)*: It calculates the average of the total power loss over all buses per time step during each episode.

We aim to find algorithms and reward functions with high CR and low PL.

MARL Algorithm Settings. We evaluate the performances of state-of-the-art MARL algorithms, i.e. IDDPG [48], MADDPG [49], COMA [50], IPPO [2], MAPPO [3], SQDDPG [48] and MATD3 [51] on this real-world problem with continuous actions. Since the original COMA can only work

for discrete actions, we conduct some modifications so that it can work for continuous actions (see Appendix B). The details of settings are shown in Appendix C.

5.2 Main Results

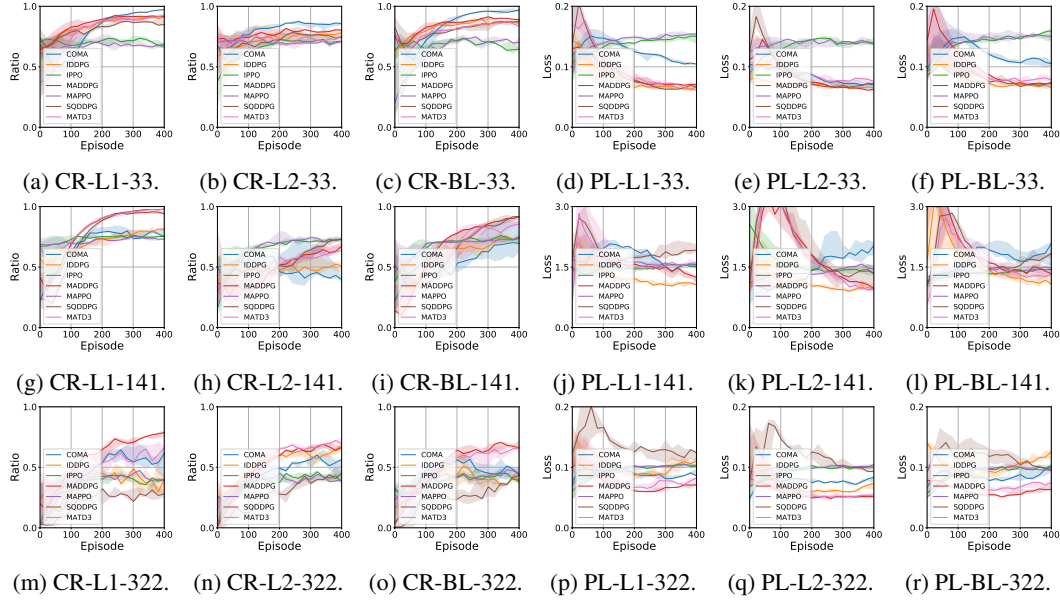


Figure 5: Median CR and PL of algorithms with different voltage barrier functions. The sub-caption indicates metric-Barrier-scenario and BL is the contraction of Bowl.

Algorithm Performances. We first show the main results of all algorithms on all scenarios in Figure 5. MADDPG and MATD3 generally perform well on all scenarios with different voltage barrier functions. COMA performs well over CR on 33-bus networks and the performances fall on the large scale scenarios, but its PL is high. Similarly, SQDDPG performs generally well over CR on 33-bus and 141-bus networks, but it performs the worst on 322-bus networks and its PL on 141-bus networks is high. This reveals the limitations of COMA and SQDDPG on the scaling to many agents. Although MAPPO and IPPO performed well on games [2, 3], their performances on the real-world power network problems are poor. The most probable reason could be that the variations of dynamics and uncertainties in distribution networks are far faster and more complicated than games and their conservative policy updates cannot fast respond. IDDPG performs at the middle place in all scenarios, which may be due to non-stationary dynamics caused by multiple agents [49].

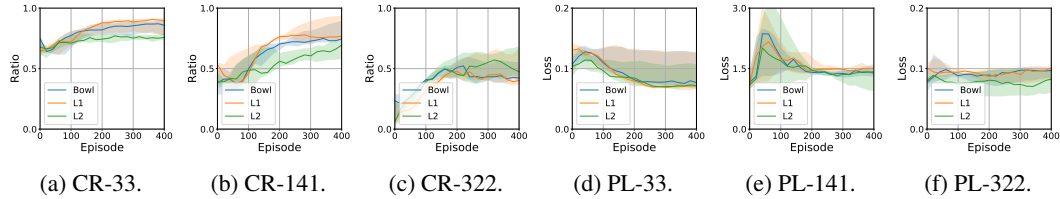


Figure 6: Median performance of overall algorithms with different voltage barrier functions. The sub-caption indicates metric-scenario.

Voltage Barrier Function Comparisons. To study the effects of different voltage barrier functions, we show the median performance of overall 7 MARL algorithms in Figure 6. It can be observed that Bowl-shape can preserve the high CR, while maintain the low PL on 33-bus and 141-bus networks. Although L1-shape can achieve the best CR on 33-bus and 141-bus networks, its PL on the 141-bus network is the highest. L2-shape performs the worst on 33-bus and 141-bus networks, but performs the best on the 322-bus network with the highest CR and the lowest PL. The reason could be that its slighter gradients is more suitable for the adaption among many agents. From the results, we can

conclude that L1-shape, Bowl-shape and L2-shape are the best choices for the 33-bus network, the 141-bus network and the 322-bus network respectively.

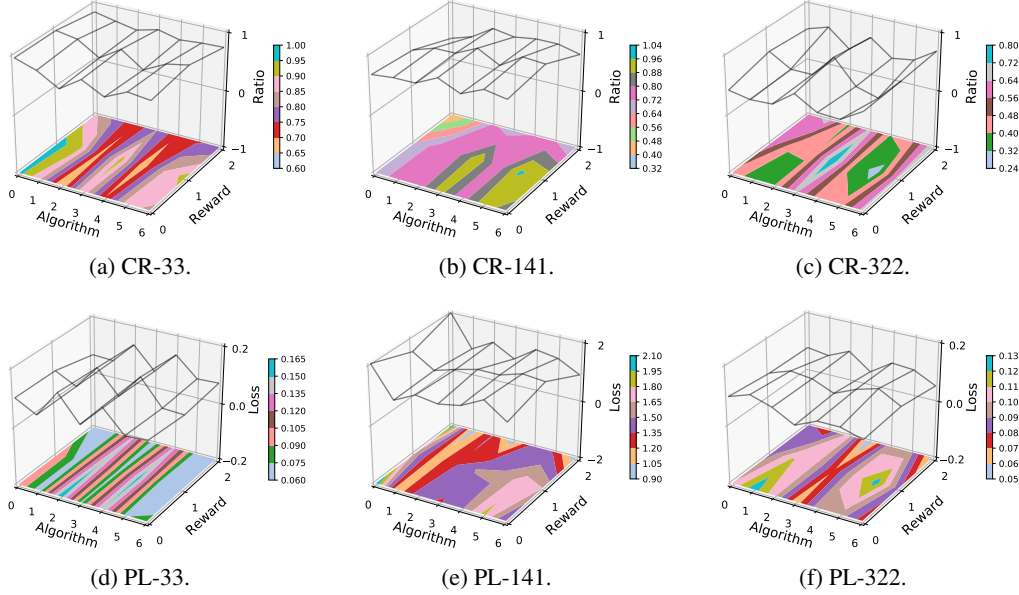


Figure 7: Median performances of overall algorithms trained with various rewards consist of distinct voltage barrier functions shown in 3D surfaces. The sub-caption indicates metric-scenario.

Diverse Algorithm Performances under Distinct Rewards. To clearly show the relationship between algorithms and reward functions, we also plot 3D surfaces over CR and PL w.r.t. algorithm types and reward types (consisting of distinct voltage barrier functions) in Figure 7. It is obvious that the performances of algorithms are highly correlated with the reward types. In other words, the same algorithm could perform diversely even trained by different reward functions with the same objective but different shapes.

5.3 Comparison between MARL and Traditional Control Methods

To compare MARL algorithms with the traditional control methods, we conduct a series of tests on various network topologies (i.e. 33-bus, 141-bus, and 322-bus networks). MADDPG trained by Bowl-shape is selected as the candidate for MARL. The traditional control methods that we select are OPF [24] and droop control [22]. For conciseness, we only demonstrate the voltages and powers on a typical bus with a PV installed (i.e. one of the most difficult buses to control) during a day (i.e. 480 consecutive time steps) in summer and winter respectively. The results for the 33-bus network is presented here and the results for other typologies are given in the Appendix E.2. From Figure 8, it can be seen that all methods control the voltage within the safety range in both summer and winter. Additionally, the power losses of MARL are lower than droop control but higher than OPF. This phenomenon is possibly due to the fact that droop control is a fully distributed algorithm which cannot explicitly reduce the power loss and OPF is a centralised algorithm with the known system model, while MARL lies between these 2 types of algorithms. This implies that MARL may outperform droop control for particular cases but it needs to be kept in mind that the droop gain used here may not be optimal. It is also worth noting that the control actions of MARL has a similar feature to droop control in the 33-bus case, and this feature is also observed in the 141-bus and 322-bus cases (see Figure 14-15 in the Appendix E.2 for details). However, this droop-like behaviour is missing in the winter case of 322-bus network, where the MARL control action is opposite to the desired direction, resulting in higher power losses and voltage deviation. This might be due to the over-generation as the MARL share the same policy for different seasons, so that it leads to the problem of relative overgeneralisation [52]. In summary, MARL seems able to learn the features of droop control but fails to outperform droop control significantly, and is even worse than droop control for certain cases.

As a result, there is still significant headroom of improvement for MARL, in performance, robustness, and interpretability.

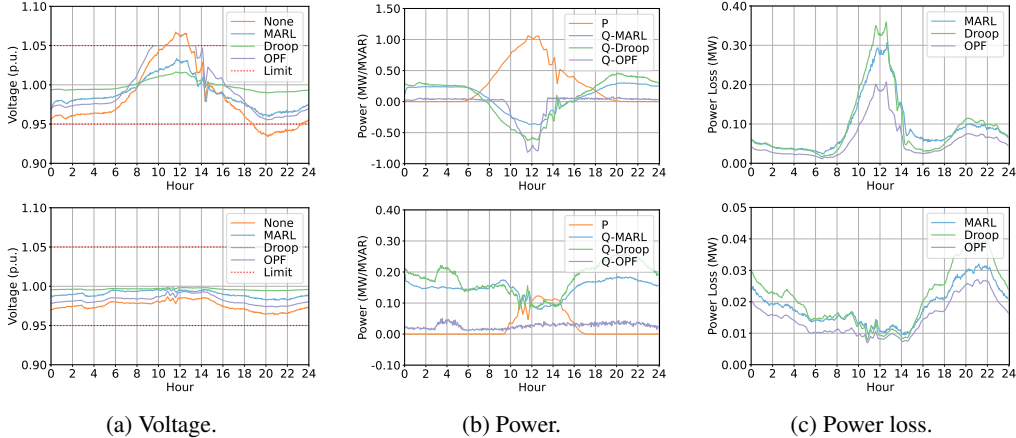


Figure 8: Compare MARL with traditional control methods on bus 18 during a day for 33-bus network. 1st row: results for a summer day. 2nd row: results for a winter day. None and limit in (a) represent the voltage with no control and the safety voltage range respectively. P and Q in (b) indicate the PV active power and the reactive power by various methods.

5.4 Discussion

We now discuss the phenomenons that we observe from the experimental results.

- It is obvious that the voltage barrier function may impact the performance of an algorithm (even with tiny changes for the common goal). This may be of general importance as many real-world problems may contain constraints that are not indirect in the objective function. An overall methodology is needed for designing barrier functions in state-constraint MARL.
- MARL may scale well for the number of agents and the complexity of networks, and only requires a very low control rate for active voltage control.
- The results above show the evidence that MARL may behave diversely from the traditional control methods. Some of the learnt behaviours may induce better performance, but some others deteriorate the performance. This shows the promising benefits of MARL in industrial applications but also highlights the drawbacks in interpretability and robustness.
- The combination of learning algorithms with domain knowledge is a potential roadmap towards interpretable MARL. For the active voltage control problem, the domain knowledge may present as network topology, inner control loops (say droop control), and load pattern. The exploitation of such domain knowledge reduces the dimensions of MARL exploration space and may offer a lower bound of performance as a guarantee. Encoding domain knowledge such as the network topology as a priori for model-based MARL is also a potential direction.

6 Conclusion

This paper investigates the potential of applying multi-agent reinforcement learning (MARL) to the active voltage control in power distribution networks. We firstly formulate this problem as a Dec-POMDP and then study the behaviours of MARL with various voltage barrier functions (reflecting voltage constraints as barrier penalties). Moreover, we compare the behaviours of MARL with the traditional control methods (i.e. droop control and OPF), and observe that MARL is possible to generate inexplicable behaviours, so an interpretable and trustable algorithm is highly desired for industrial applications. Finally, the environment used in this work is open-sourced and easy to follow so that the machine learning community is able to contribute to this challenging real-world problem.

Acknowledgement

This work is supported by the Engineering and Physical Sciences Research Council of UK (EPSRC) under awards EP/S000909/1.

References

- [1] David Silver, Julian Schrittwieser, Karen Simonyan, Ioannis Antonoglou, Aja Huang, Arthur Guez, Thomas Hubert, Lucas Baker, Matthew Lai, Adrian Bolton, et al. Mastering the game of go without human knowledge. *nature*, 550(7676):354–359, 2017.
- [2] Christian Schroeder de Witt, Tarun Gupta, Denys Makoviichuk, Viktor Makoviychuk, Philip HS Torr, Mingfei Sun, and Shimon Whiteson. Is independent learning all you need in the starcraft multi-agent challenge? *arXiv preprint arXiv:2011.09533*, 2020.
- [3] Chao Yu, Akash Velu, Eugene Vinitzky, Yu Wang, Alexandre Bayen, and Yi Wu. The surprising effectiveness of mappo in cooperative, multi-agent games. *arXiv preprint arXiv:2103.01955*, 2021.
- [4] Christian Schroeder de Witt, Bei Peng, Pierre-Alexandre Kamienny, Philip Torr, Wendelin Böhmer, and Shimon Whiteson. Deep multi-agent reinforcement learning for decentralized continuous cooperative control. *arXiv preprint arXiv:2003.06709*, 2020.
- [5] Dawei Qiu, Jianhong Wang, Junkai Wang, and Goran Strbac. Multi-agent reinforcement learning for automated peer-to-peer energy trading in double-side auction market. In Zhi-Hua Zhou, editor, *Proceedings of the Thirtieth International Joint Conference on Artificial Intelligence, IJCAI 2021, Virtual Event / Montreal, Canada, 19-27 August 2021*, pages 2913–2920. ijcai.org, 2021.
- [6] Di Cao, Weihao Hu, Junbo Zhao, Guozhou Zhang, Bin Zhang, Zhou Liu, Zhe Chen, and Frede Blaabjerg. Reinforcement learning and its applications in modern power and energy systems: A review. *Journal of Modern Power Systems and Clean Energy*, 8(6):1029–1042, 2020. doi: 10.35833/MPCE.2020.000552.
- [7] Efstratios Batzelis, Zakir Hussain Rather, John Barton, Bonu Ramesh Naidu, Billy Wu, Firdous UI Nazir, ONYEMA SUNDAY NDUKA, Wei He, Jerome Nsengiyaremye, and Bandopant Pawar. Solar integration in the uk and india: technical barriers and future directions. *Report of the UK-India Joint Virtual Clean Energy Centre (JVCEC)*, 2021.
- [8] Reinaldo Tonkoski, Dave Turcotte, and Tarek H. M. EL-Fouly. Impact of high pv penetration on voltage profiles in residential neighborhoods. *IEEE Transactions on Sustainable Energy*, 3(3):518–527, 2012. doi: 10.1109/TSTE.2012.2191425.
- [9] Pedro MS Carvalho, Pedro F Correia, and Luís AFM Ferreira. Distributed reactive power generation control for voltage rise mitigation in distribution networks. *IEEE transactions on Power Systems*, 23(2):766–772, 2008.
- [10] Tomonobu Senjyu, Yoshitaka Miyazato, Atsushi Yona, Naomitsu Urasaki, and Toshihisa Funabashi. Optimal distribution voltage control and coordination with distributed generation. *IEEE Transactions on Power Delivery*, 23(2):1236–1242, 2008. doi: 10.1109/TPWRD.2007.908816.
- [11] Konstantin Turitsyn, Petr Sulc, Scott Backhaus, and Michael Chertkov. Options for control of reactive power by distributed photovoltaic generators. *Proceedings of the IEEE*, 99(6):1063–1073, 2011. doi: 10.1109/JPROC.2011.2116750.
- [12] Johanna Barr and Ritwik Majumder. Integration of distributed generation in the volt/var management system for active distribution networks. *IEEE Transactions on Smart Grid*, 6(2):576–586, 2015. doi: 10.1109/TSG.2014.2363051.
- [13] Di Cao, Junbo Zhao, Weihao Hu, Fei Ding, Qi Huang, and Zhe Chen. Distributed voltage regulation of active distribution system based on enhanced multi-agent deep reinforcement learning. *arXiv preprint arXiv:2006.00546*, 2020.

- [14] Di Cao, Weihao Hu, Junbo Zhao, Qi Huang, Zhe Chen, and Frede Blaabjerg. A multi-agent deep reinforcement learning based voltage regulation using coordinated pv inverters. *IEEE Transactions on Power Systems*, 35(5):4120–4123, 2020.
- [15] Di Cao, Junbo Zhao, Weihao Hu, Fei Ding, Qi Huang, Zhe Chen, and Frede Blaabjerg. Data-driven multi-agent deep reinforcement learning for distribution system decentralized voltage control with high penetration of pvs. *IEEE Transactions on Smart Grid*, 2021.
- [16] Haotian Liu and Wenchuan Wu. Online multi-agent reinforcement learning for decentralized inverter-based volt-var control. *IEEE Transactions on Smart Grid*, 2021.
- [17] Frans A Oliehoek and Christopher Amato. *A concise introduction to decentralized POMDPs*. Springer, 2016.
- [18] C.L. Masters. Voltage rise: the big issue when connecting embedded generation to long 11 kv overhead lines. *Power Engineering Journal*, 16(1):5–12, 2002. doi: 10.1049/pe:20020101.
- [19] Giuseppe Fusco and Mario Russo. A decentralized approach for voltage control by multiple distributed energy resources. *IEEE Transactions on Smart Grid*, pages 1–1, 2021. doi: 10.1109/TSG.2021.3057546.
- [20] Yashodhan P. Agalgaonkar, Bikash C. Pal, and Rabih A. Jabr. Distribution voltage control considering the impact of pv generation on tap changers and autonomous regulators. *IEEE Transactions on Power Systems*, 29(1):182–192, 2014. doi: 10.1109/TPWRS.2013.2279721.
- [21] Panagis N. Vovos, Aristides E. Kiprakis, A. Robin Wallace, and Gareth P. Harrison. Centralized and distributed voltage control: Impact on distributed generation penetration. *IEEE Transactions on Power Systems*, 22(1):476–483, 2007. doi: 10.1109/TPWRS.2006.888982.
- [22] Pedram Jahangiri and Dionysios C. Aliprantis. Distributed volt/var control by pv inverters. *IEEE Transactions on Power Systems*, 28(3):3429–3439, 2013. doi: 10.1109/TPWRS.2013.2256375.
- [23] Johannes Schiffer, Thomas Seel, Jörg Raisch, and Tevfik Sezi. Voltage stability and reactive power sharing in inverter-based microgrids with consensus-based distributed voltage control. *IEEE Transactions on Control Systems Technology*, 24(1):96–109, 2016. doi: 10.1109/TCST.2015.2420622.
- [24] Lingwen Gan, Na Li, Ufuk Topcu, and Steven H Low. Optimal power flow in tree networks. In *52nd IEEE Conference on Decision and Control*, pages 2313–2318. IEEE, 2013.
- [25] Yan Xu, Zhao Yang Dong, Rui Zhang, and David J Hill. Multi-timescale coordinated voltage/var control of high renewable-penetrated distribution systems. *IEEE Transactions on Power Systems*, 32(6):4398–4408, 2017.
- [26] Emiliano Dall’Anese, Sairaj V. Dhople, and Georgios B. Giannakis. Optimal dispatch of photovoltaic inverters in residential distribution systems. *IEEE Transactions on Sustainable Energy*, 5(2):487–497, 2014. doi: 10.1109/TSTE.2013.2292828.
- [27] Weiye Zheng, Wenchuan Wu, Boming Zhang, Hongbin Sun, and Yibing Liu. A fully distributed reactive power optimization and control method for active distribution networks. *IEEE Transactions on Smart Grid*, 7(2):1021–1033, 2016. doi: 10.1109/TSG.2015.2396493.
- [28] Zhiyuan Tang, David J Hill, and Tao Liu. Distributed coordinated reactive power control for voltage regulation in distribution networks. *IEEE Transactions on Smart Grid*, 12(1):312–323, 2020.
- [29] Hongbin Sun, Qinglai Guo, Junjian Qi, Venkataramana Ajjarapu, Richard Bravo, Joe Chow, Zhengshuo Li, Rohit Moghe, Ehsan Nasr-Azadani, Ujjwol Tamrakar, Glauco N. Taranto, Reinaldo Tonkoski, Gustavo Valverde, Qiuwei Wu, and Guangya Yang. Review of challenges and research opportunities for voltage control in smart grids. *IEEE Transactions on Power Systems*, 34(4):2790–2801, 2019. doi: 10.1109/TPWRS.2019.2897948.
- [30] Ankit Singhal, Venkataramana Ajjarapu, Jason Fuller, and Jacob Hansen. Real-time local volt/var control under external disturbances with high pv penetration. *IEEE Transactions on Smart Grid*, 10(4):3849–3859, 2019. doi: 10.1109/TSG.2018.2840965.

- [31] Mehdi Zeraati, Mohamad Esmail Hamedani Golshan, and Josep M Guerrero. Voltage quality improvement in low voltage distribution networks using reactive power capability of single-phase pv inverters. *IEEE transactions on smart grid*, 10(5):5057–5065, 2018.
- [32] Shengyi Wang, Jiajun Duan, Di Shi, Chunlei Xu, Haifeng Li, Ruisheng Diao, and Zhiwei Wang. A data-driven multi-agent autonomous voltage control framework using deep reinforcement learning. *IEEE Transactions on Power Systems*, 35(6):4644–4654, 2020.
- [33] Scott Burger, Jesse D Jenkins, Carlos Batlle López, and José Ignacio Pérez Arriaga. Restructuring revisited: competition and coordination in electricity distribution systems. 2018.
- [34] Marvin Lerousseau. Design and implementation of an environment for learning to run a power network (l2rpn). *arXiv preprint arXiv:2104.04080*, 2021.
- [35] Robin Henry and Damien Ernst. Gym-ann: Reinforcement learning environments for active network management tasks in electricity distribution systems. *Energy and AI*, page 100092, 2021.
- [36] Leon Thurner, Alexander Scheidler, Florian Schäfer, Jan-Hendrik Menke, Julian Dollichon, Friederike Meier, Steffen Meinecke, and Martin Braun. Pandapower—an open-source python tool for convenient modeling, analysis, and optimization of electric power systems. *IEEE Transactions on Power Systems*, 33(6):6510–6521, 2018. doi: 10.1109/TPWRS.2018.2829021.
- [37] Steffen Meinecke, Džanan Sarajlić, Simon Ruben Drauz, Annika Klettke, Lars-Peter Lauen, Christian Rehtanz, Albert Moser, and Martin Braun. Simbench—a benchmark dataset of electric power systems to compare innovative solutions based on power flow analysis. *Energies*, 13(12), 2020. ISSN 1996-1073. URL <https://www.mdpi.com/1996-1073/13/12/3290>.
- [38] Hadi Saadat et al. *Power system analysis*, volume 2. McGraw-hill, 1999.
- [39] Yashodhan P Agalgaonkar, Bikash C Pal, and Rabih A Jabr. Distribution voltage control considering the impact of pv generation on tap changers and autonomous regulators. *IEEE Transactions on Power Systems*, 29(1):182–192, 2013.
- [40] Guangya Yang, Francesco Marra, Miguel Juamperez, Søren Bækthøj Kjær, Seyedmostafa Hashemi, Jacob Østergaard, Hans Henrik Ipsen, and Kenn H. B. Frederiksen. Voltage rise mitigation for solar pv integration at lv grids studies from pvnet. dk. *Journal of Modern Power Systems and Clean Energy*, 3(3):411–421, 2015. doi: 10.1007/s40565-015-0132-0.
- [41] Antonio Gómez-Expósito, Antonio J Conejo, and Claudio Cañizares. *Electric energy systems: analysis and operation*. CRC press, 2018.
- [42] Ieee standard for interconnection and interoperability of distributed energy resources with associated electric power systems interfaces. *IEEE Std 1547-2018 (Revision of IEEE Std 1547-2003)*, pages 1–138, 2018. doi: 10.1109/IEEESTD.2018.8332112.
- [43] Irina Higgins, Loic Matthey, Arka Pal, Christopher Burgess, Xavier Glorot, Matthew Botvinick, Shakir Mohamed, and Alexander Lerchner. beta-vae: Learning basic visual concepts with a constrained variational framework. 2016.
- [44] M.E. Baran and F.F. Wu. Network reconfiguration in distribution systems for loss reduction and load balancing. *IEEE Transactions on Power Delivery*, 4(2):1401–1407, 1989. doi: 10.1109/61.25627.
- [45] H.M. Khodr, F.G. Olsina, P.M. De Oliveira-De Jesus, and J.M. Yusta. Maximum savings approach for location and sizing of capacitors in distribution systems. *Electric Power Systems Research*, 78(7):1192–1203, 2008. ISSN 0378-7796. doi: <https://doi.org/10.1016/j.epsr.2007.10.002>. URL <https://www.sciencedirect.com/science/article/pii/S0378779607002143>.
- [46] Ray Daniel Zimmerman, Carlos Edmundo Murillo-Sánchez, and Robert John Thomas. Matpower: Steady-state operations, planning, and analysis tools for power systems research and education. *IEEE Transactions on power systems*, 26(1):12–19, 2010.

- [47] Rajiv K. Varma and Ehsan M. Siavashi. Pv-statcom: A new smart inverter for voltage control in distribution systems. *IEEE Transactions on Sustainable Energy*, 9(4):1681–1691, 2018. doi: 10.1109/TSTE.2018.2808601.
- [48] Jianhong Wang, Yuan Zhang, Tae-Kyun Kim, and Yunjie Gu. Shapley q-value: A local reward approach to solve global reward games. *Proceedings of the AAAI Conference on Artificial Intelligence*, 34(05):7285–7292, Apr 2020.
- [49] Ryan Lowe, Yi Wu, Aviv Tamar, Jean Harb, Pieter Abbeel, and Igor Mordatch. Multi-agent actor-critic for mixed cooperative-competitive environments. In Isabelle Guyon, Ulrike von Luxburg, Samy Bengio, Hanna M. Wallach, Rob Fergus, S. V. N. Vishwanathan, and Roman Garnett, editors, *Advances in Neural Information Processing Systems 30: Annual Conference on Neural Information Processing Systems 2017, December 4-9, 2017, Long Beach, CA, USA*, pages 6379–6390, 2017.
- [50] Jakob N Foerster, Gregory Farquhar, Triantafyllos Afouras, Nantas Nardelli, and Shimon Whiteson. Counterfactual multi-agent policy gradients. In *Thirty-Second AAAI Conference on Artificial Intelligence*, 2018.
- [51] Johannes Ackermann, Volker Gabler, Takayuki Osa, and Masashi Sugiyama. Reducing overestimation bias in multi-agent domains using double centralized critics. *arXiv preprint arXiv:1910.01465*, 2019.
- [52] Ermo Wei and Sean Luke. Lenient learning in independent-learner stochastic cooperative games. *The Journal of Machine Learning Research*, 17(1):2914–2955, 2016.
- [53] Rajiv K. Varma, V. Khadkikar, and Ravi Seethapathy. Nighttime application of pv solar farm as statcom to regulate grid voltage. *IEEE Transactions on Energy Conversion*, 24(4):983–985, 2009. doi: 10.1109/TEC.2009.2031814.
- [54] Scott Fujimoto, Herke Hoof, and David Meger. Addressing function approximation error in actor-critic methods. In *International Conference on Machine Learning*, pages 1587–1596. PMLR, 2018.
- [55] Tuomas Haarnoja, Aurick Zhou, Kristian Hartikainen, George Tucker, Sehoon Ha, Jie Tan, Vikash Kumar, Henry Zhu, Abhishek Gupta, Pieter Abbeel, et al. Soft actor-critic algorithms and applications. *arXiv preprint arXiv:1812.05905*, 2018.
- [56] Jimmy Lei Ba, Jamie Ryan Kiros, and Geoffrey E Hinton. Layer normalization. *arXiv preprint arXiv:1607.06450*, 2016.
- [57] Junyoung Chung, Caglar Gulcehre, KyungHyun Cho, and Yoshua Bengio. Empirical evaluation of gated recurrent neural networks on sequence modeling. *arXiv preprint arXiv:1412.3555*, 2014.
- [58] Tijmen Tieleman and Geoffrey Hinton. Lecture 6.5-rmsprop: Divide the gradient by a running average of its recent magnitude. *COURSERA: Neural networks for machine learning*, 4(2): 26–31, 2012.
- [59] John Schulman, Philipp Moritz, Sergey Levine, Michael I. Jordan, and Pieter Abbeel. High-dimensional continuous control using generalized advantage estimation. In Yoshua Bengio and Yann LeCun, editors, *4th International Conference on Learning Representations, ICLR 2016, San Juan, Puerto Rico, May 2-4, 2016, Conference Track Proceedings*, 2016.
- [60] Yuanyuan Chai, Li Guo, Chengshan Wang, Zongzheng Zhao, Xiaofeng Du, and Jing Pan. Network partition and voltage coordination control for distribution networks with high penetration of distributed pv units. *IEEE Transactions on Power Systems*, 33(3):3396–3407, 2018. doi: 10.1109/TPWRS.2018.2813400.
- [61] Maryam Majzoubi, Chicheng Zhang, Rajan Chari, Akshay Krishnamurthy, John Langford, and Aleksandrs Slivkins. Efficient contextual bandits with continuous actions. In Hugo Larochelle, Marc’Aurelio Ranzato, Raia Hadsell, Maria-Florina Balcan, and Hsuan-Tien Lin, editors, *Advances in Neural Information Processing Systems 33: Annual Conference on Neural Information Processing Systems 2020, NeurIPS 2020, December 6-12, 2020, virtual*, 2020.

A Additional Background of Voltage Control Problem

A.1 Power Flow Problem

Recall the power balance equations:

$$\begin{aligned} p_i^{PV} - p_i^L &= v_i^2 \sum_{j \in V_i} g_{ij} - v_i \sum_{j \in V_i} v_j (g_{ij} \cos \theta_{ij} + b_{ij} \sin \theta_{ij}), \quad \forall i \in V \setminus \{0\} \\ q_i^{PV} - q_i^L &= -v_i^2 \sum_{j \in V_i} b_{ij} + v_i \sum_{j \in V_i} v_j (g_{ij} \sin \theta_{ij} + b_{ij} \cos \theta_{ij}), \quad \forall i \in V \setminus \{0\} \end{aligned} \quad (3)$$

The power flow problem is designed to find the steady-state operation point of power system. After measuring power injections $p_i^{PV} - p_i^L$ and $q_i^{PV} - q_i^L$, the bus voltages $v_i \angle \theta_i$ can be retrieved by iteratively solving Eq.3 using Newton-Raphson or Gauss-Seidel method [41]. The power flow serves as the fundamental role in grid planning and security assessment by locating any voltage deviations. It is also used to generate the observations during MARL training.

A.2 Voltage Deviation and Control

Two-Bus Network. To intuitively show how voltage is varied by PVs and how PV inverters can participate in voltage control, we give an example for a two-bus distribution network in Figure 9. In Figure 9, $z_i = r_i + jx_i$ represents the impedance on branch i ; r_i and x_i are resistance and reactance on branch i , respectively; p_i^L and q_i^L denote active and reactive power consumption, respectively; p_i^{PV} and q_i^{PV} indicate active and reactive PV power generation, respectively. The parent bus voltage v_{i_p} is set as reference for the two-bus network.

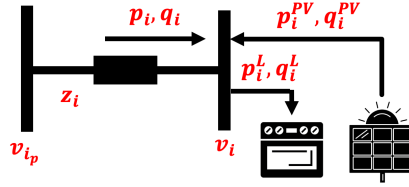


Figure 9: Two-bus electric circuit of the distribution network.

The voltage drop $\Delta v_i = v_{i_p} - v_i$ in Figure 9 can be approximated as follows:

$$\Delta v_i = \frac{r_i(p_i^L - p_i^{PV}) + x_i(q_i^L - q_i^{PV})}{v_i} \quad (4)$$

The power loss of the 2-bus network in Figure 9 can be written as:

$$P_{\text{loss}} = \frac{(p_i^L - p_i^{PV})^2 + (q_i^L - q_i^{PV})^2}{v_{i_p}^2} \cdot r_i \quad (5)$$

Traditional Voltage Control Methods. Conventionally, PVs are not allowed to participate in voltage control so that q_i^{PV} is restricted to 0 by the grid code. To export its power, large penetration of p_i^{PV} may increase v_i out of its safe range, causing reverse current flow [18, 40]. Voltage control devices, such as shunt capacitor (SC) and step voltage regulator (SVR) are usually equipped in the network to maintain the voltage level [10]. Nonetheless, these methods cannot respond to intermittent solar radiation, e.g. frequent voltage fluctuation due to cloud cover [30]. Additionally, with the rising PV penetration in the network, the operation of traditional regulators would be at their control limit (i.e. runaway condition) [20].

Inverter-based Volt/Var Control. To adapt to the continually rising PV penetration, grid-support services, such as voltage and reactive power control are required for every new-installed PV by the latest grid code IEEE Std-1547™-2018 [42]. For instance, the PV reactive power can be regulated by the PV-inverter under partial static synchronous compensator (STATCOM) mode [47]. Depending

on the voltage deviation levels, the inverter can inject or absorb different amount of reactive power exceeding its capacity [53]. This control method is then named as Volt/Var control, as the reactive power (with unit VAR) is determined by the voltage (with unit Volt). Intuitively by Eq.4, when the voltage increases due to large PV penetration in the lunch-time, the PV inverter absorbs reactive power while during the night-time, the full inverter capacity is used to balance voltage fluctuation caused by increasing load [20].

Note that the only control variable in Eq.4 and Eq.5 is q_i^{PV} which represents the reactive power generated by PV. Based on Eq.4, to enforce zero voltage deviation, the reactive power should satisfy the following condition

$$q_i^{PV} = \frac{r_i}{x_i}(p_i^L - p_i^{PV}) + q_i^L \quad (6)$$

Since the ratio r_i/x_i in the distribution network is extremely large, q_i^{PV} could become negative (i.e. absorbing reactive power) with great magnitude during the period of the peak PV injection (i.e., $p_i^{PV} \gg p_i^L$).

From Eq.5, to achieve the least power loss, q_i^{PV} needs to be equal to q_i^L (i.e. no reactive power injection). This result may conflict with the voltage control target in Eq.6, implying that it is hard to simultaneously maintain safe voltage levels and minimise the power losses, even for the two-bus network.

This section only demonstrates a 2-bus network which has linear relationship between voltage deviation and PV reactive power. Although the power systems in real world are non-linear and more complex, they are with the same phenomenon on the contradiction between voltage control and power loss minimisation.

A.3 Optimal Power Flow

The optimal power flow (OPF) considered in this paper can be briefly formulated as:

$$\begin{aligned} \min_{q_i^{PV}} \quad & p_0 \\ \text{s.t.} \quad & \text{Eq.1} \\ & |q_i^{PV}| \leq q_{i,\max}^{PV}, \quad i \in V^{PV} \\ & v_{i,\min} \leq v_i \leq v_{i,\max}, \quad i \in V \setminus 0 \\ & v_0 = v_{\text{ref}} \end{aligned} \quad (7)$$

where p_0 and v_0 are the active power and reference voltage of the slack bus, respectively. V^{PV} is the index set of the buses equipped with PVs. p_i^{PV} , q_i^{PV} , and s_i are the active power, reactive power, and the capacity of PV at bus i , respectively. In this paper, each PV inverter is oversized with $s_i = 1.2 p_{i,\max}$, $\forall i \in V^{PV}$. The maximum PV reactive power is $q_{i,\max}^{PV} = \sqrt{s_i^2 - (p_i^{PV})^2}$. Note that the objective of the OPF problem is equivalent to minimize the overall power loss.

Eq.7 may be infeasible due to the large penetration of PVs. In this case, slack variables can be added on the voltage constraint.

A.4 Droop Control

The droop control, as recommended by IEEE Std-1547TM-2018 [42], follows the control strategy $q_i^{PV} = f(v_i)$ where q_i^{PV} and v_i are the PV reactive power and the voltage measurement of a PV bus i . $f(\cdot)$ is piecewise linear as shown in Figure 10. In detail, v_{ref} represents the voltage set point (e.g. 1.0 p.u.). v_a and v_d represent the saturation regions limited by the PV inverter capacity and the current PV active power. There also exists a dead-band between v_b and v_c that does not require any control. For the voltage lower than v_b , the inverter provides reactive power proportional to the voltage deviation against v_{ref} . If the voltage is higher than v_c , the inverter absorbs reactive power until convergence achieves. The droop control only requires the local voltage measurements that is simple and efficient to implement. However, it cannot directly minimise the power losses nor respond to fast voltage changes. For simplicity, we set $v_b = v_c = v_{\text{ref}}$ in this work.

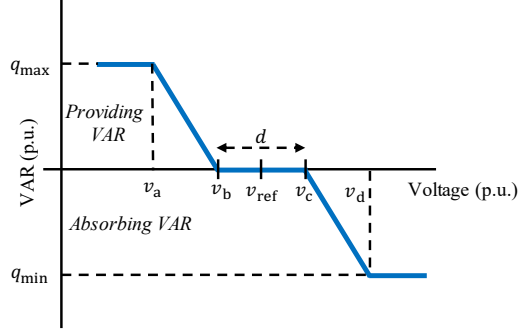


Figure 10: The illustration of the droop control law.

B COMA with Continuous Actions

COMA [50] is an MARL algorithm with credit assignments over Q-value functions via the mechanism of counterfactual regret, however, it can only serve for the discrete action space. In this paper, to enable COMA eligible for the continuous action space, we conduct some tiny adjustments on the construction of Q-value for each agent. The original version of calculating each agent’s Q-value assignment w.r.t. the discrete actions is shown as follows:

$$Q_i(\mathbf{s}, \mathbf{a}) = Q(\mathbf{s}, \mathbf{a}) - \sum_{a'_i \in \mathcal{A}_i} \pi_i(a'_i | \tau_i) Q(\mathbf{s}, \mathbf{a}_{-i}, a'_i), \quad (8)$$

where τ_i is a history of agent i ; $\mathbf{a}_{-i} = \times_{j \neq i} a_j$. To fit the continuous actions, we simply change Eq.8 to the form such that

$$Q_i(\mathbf{s}, \mathbf{a}) = Q(\mathbf{s}, \mathbf{a}) - \int_{a'_i \in \mathcal{A}_i} Q(\mathbf{s}, \mathbf{a}_{-i}, a'_i) d\pi_i(a'_i | \tau_i), \quad (9)$$

where $\pi_i(a'_i | \tau_i)$ is a Gaussian distribution over a'_i . In practice, $\int_{a'_i \in \mathcal{A}_i} Q(\mathbf{s}, \mathbf{a}_{-i}, a'_i) d\pi_i(a'_i | \tau_i)$ is approximated via Monte Carlo sampling, so it can be written as follows:

$$Q_i(\mathbf{s}, \mathbf{a}) = Q(\mathbf{s}, \mathbf{a}) - \frac{1}{M} \sum_{k=1}^M Q(\mathbf{s}, \mathbf{a}_{-i}, (a'_i)_k), \quad (a'_i)_k \sim \pi_i(a'_i | \tau_i). \quad (10)$$

C Experimental Settings

The source code of experimentation will be released after acceptance of paper for the easy reproductions and further studies.

C.1 Algorithm Settings and Training Details

Since IDDPG and MADDPG do not possess any extra hyperparameters, we only introduce the hyperparameters of COMA, MATD3, SQDDPG, IPPO, and MAPPO that we used in experiments.

Common Settings. All algorithms are trained with online learning (i.e., for the on-policy algorithms like IPPO and MAPPO the behaviour policies are updated once at the end of each episode; for the on-policy algorithm like COMA the behaviour policies/values are updated every 60 time steps; and for the off-policy algorithms like SQDDPG, IDDPG and MADDPG the behaviour policies/values are updated every 60 time steps, where all data used for training are collected online) and the target policy/critic networks are updated every interval that is twice as the update interval of behaviour policy/critic introduced above. Taking the lessons from [48, 54], the algorithms except for MAPPO and IPPO update critic networks with 10 epochs while update policy networks with 1 epoch. All algorithms are trained with the normalised reward and the action bound enforcement trick [55] that works better than the hard clipping in our experiments. The target update learning rate is set to 0.1. The gradient is clipped with L1 norm and the clip bound is set to 1. The batch size of training data is

set to 32 and the replay buffer size for off-policy algorithms is set to 5,000. Agent ID is concatenated with the observation and the layer normalisation [56] is applied to the first layer after the observation input. The parameters are shared among agents in this experiment. As for the policy network, RNN with GRUs [57] is applied as a filter to solve the partial observation problems. The critic network is constructed with pure MLPs. The general settings of the policy and critic networks are shown in Table 1. During training, a fixed standard deviation as 1.0 is applied to conduct the exploration. For the policy loss with entropy, the entropy penalty is set to 1e-3. The parameter initialisation is implemented by sampling from normal distribution with $\mathcal{N}(0, 0.1)$. RMSProp [58] is used as the optimizer, with the learning rate of 1e-4 for updating both policies and critics.

COMA. The sample size M of COMA for continuous actions proposed in this paper is set to 10 in experiments.

MATD3. The clip boundary c for clipping the exploration noise is set to 1 in experiments.

SQDDPG. The sample size M of SQDDPG is set to 10 in experiments.

IPPO and MAPPO. We apply generalised advantage estimation (GAE) [59] to evaluate the return with $\lambda = 0.95$. The value loss coefficient is set to 2. The ϵ for clipping the objective function is set to 0.4. We also normalise the advantages during training to reduce variance. 10 epochs of training are conducted for each time of update.

All hyperparameters reported above are tuned by the grid search and the best ones are selected as the final choices.

Table 1: The general specifications for policy and value networks.

NETWORK	STRUCTURE
POLICY	LINEAR(STATE_DIM, 64) → LAYERNORM() → RELU() → GRU(64, 64) → LINEAR(64, ACTION_DIM)
CRITIC	LINEAR(INPUT_DIM, 64) → LAYERNORM() → RELU() → LINEAR(STATE_DIM, 64) → RELU() → LINEAR(64, OUTPUT_DIM)

In addition to the training details introduced in the main part of paper, we expose more in this section. At the initial state we randomly sample reactive power of generators so that the experiments are more realistic, i.e. to test whether the agents can solve any emergent situations. The training time varies from 2.5 to 4 hrs, dependent on the selection of scenarios and algorithms.

C.2 Process of Simulations

We show the flow chart in Figure 11 to illustrate the process of the execution of the simulation for distributed active voltage control on power distribution networks. At the beginning of each episode, a series of consecutive PV and load profiles for 480 time steps (i.e. 1 day) is in buffer. For each time step, the relevant PV and load profile are extracted, combined with the voltage status computed by Pandapower [36] (i.e., the power flow is calculated) to form the next state. Additionally, the reward is also calculated according to the results computed by Pandapower. Before fed to agents, the received state will be split to a batch of observations as per the region where each agent is located. Each agent only receives a local observation and the global reward, then it makes next decision. The above procedure is repeated until the end of an episode.

C.3 Voltage Barrier Functions

In this paper, we compare 3 different voltage barrier functions applied in this work. The L1-shape can be written as follows:

$$l_v(v_k) = |v_k - v_{\text{ref}}|, \quad \forall k \in V. \quad (11)$$

The L2-shape can be written as follows:

$$l_v(v_k) = (v_k - v_{\text{ref}})^2, \quad \forall k \in V. \quad (12)$$

The Bowl-shape can be written as follows:

$$l_v(v_k) = \begin{cases} a \cdot |v_k - v_{\text{ref}}| - b & \text{If } |v_k - v_{\text{ref}}| > 0.05, \\ -c \cdot \mathcal{N}(v_k | v_{\text{ref}}, 0.1) + d & \text{Otherwise,} \end{cases} \quad (13)$$

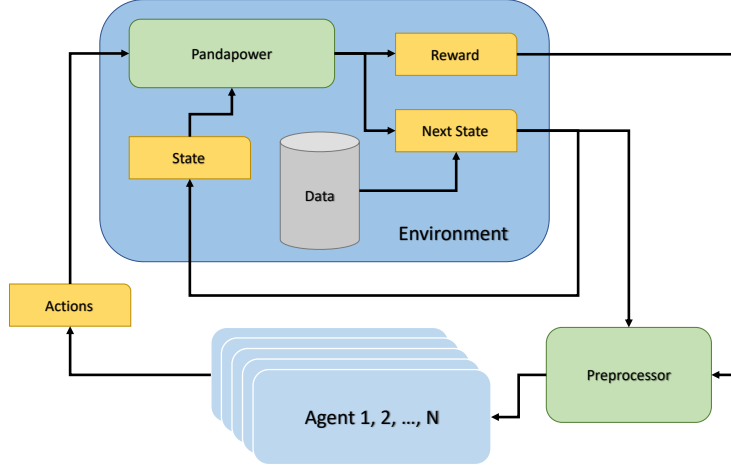


Figure 11: The flow chart of the implementation of environment for distributed active voltage control on power distribution networks.

where a, b, c, d are 4 hyperparameters to adjust the shape and smoothness of function that are set to 2, 0.095, 0.01, 0.04 respectively in this work; $\mathcal{N}(v_k | v_{\text{ref}}, 0.1)$ is a density function for the normal distribution with the mean as v_{ref} and the standard deviation as 0.1. In addition to the significance of satisfying the objective of active voltage control, this construction can also be interpreted as a sort of statistical implication. v_k is assumed to follow the Laplace distribution outside the safety range while it is assumed to follow the normal distribution inside the safety range. Thereafter, the active voltage control problem can be transformed to the maximum likelihood estimation (MLE) over a mixture distribution of voltage with a constraint on reactive power generations.

C.4 Reward for the Safety of Power Networks

Although the action range has been restricted to avoid the violence of the loading capacity of power networks, in experiments there still exists possibilities that this accident could happen. To resolve this problem, if the violence of the loading capacity appears, the system would backtrack to the last state as well as terminate the simulation and give a penalty of -200 as the reward instead of the one shown in the main part of paper.

D Environmental Settings

We present 3 MV/LV distribution network models, each of which is composed of distinct topology and parameters, a load profile (including both active and reactive powers) describing different user behaviours, and a PV profile describing the active power generation from PVs. Although it is possible to partition the control regions by the voltage sensitivity of each bus [60], they are commonly determined by different distribution network owners in practice. Consequently, the control regions in this paper are partitioned by the shortest path between the coupling bus and the terminal bus. Besides, each region consists of 1-4 PVs depending on the zonal sizes.

D.1 Network Topology

A summary of the 3 networks is recorded in Table 2 and the specific topologies are demonstrated in Figure 12.

33-bus. The 33-bus network is modified from case33bw in MATPOWER [46] and PandaPower [36]. To guarantee the tree structure, similar to [16], we drop lines 33-37 to avoid any loops. 6 PVs are added unevenly on bus 13 and 18 (zone 1), bus 22 (zone 2), bus 25 (zone 3), bus 29 and 33 (zone 4). The PV-load ratio is $PR = 2.5$.

141-bus. The 141-bus network is modified from case141 in MATPOWER [46] as well. A similar procedure is followed as 33-bus network.

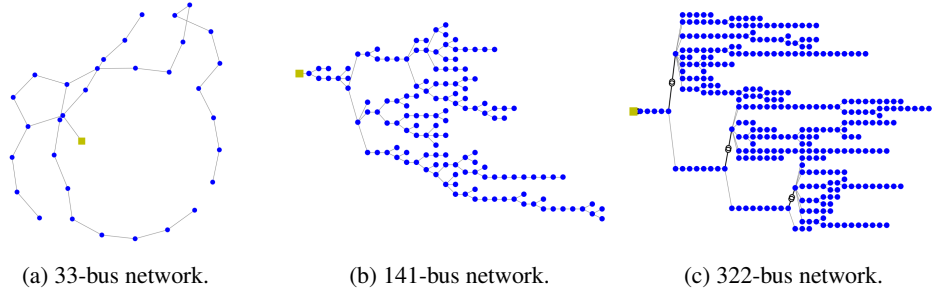


Figure 12: Topologies of power networks. The yellow square is the reference bus (a.k.a. the slack bus) and each blue circle is a non-reference bus. Transformers are highlighted as double-circles.

Table 2: Network specifications

	Rated Voltage	No. Loads	No. Regions	No. PVs	p_{\max}^L	p_{\max}^{PV}
33-bus	12.66 kV	32	4	6	3.5 MW	8.75 MW
141-bus	12.5 kV	84	9	22	20 MW	80 MW
322-bus	110-20-0.4 kV	337	22	38	1.5 MW	3.75 MW

322-bus. The proposed 322-bus network consists of an external 110-kV bus, a long medium-voltage (20 kV) line (25 buses in total) and 3 LV feeders (0.4 kV) representing rural (128 buses), semi-urban (110 buses), and urban (58 buses) areas defined by SimBench [37]. Areas with different voltage levels are connected through standard transformers defined in PandaPower [36]. The rural area has the lowest power consumption level and some buses are with no loads, while more than one load are allowed to locate on a bus in the urban area, so the total number of loads is higher than the number of buses in the 322-bus network. The users can also generate their own synthetic networks by following our procedure. To simplify the settings, we aggregate the multiple loads at each bus into one.

D.2 Data Descriptions.

Load Profiles. The load profile of each network is modified based on the real-time Portuguese electricity consumption accounting for 232 consumers of 3 years.⁹ The original dataset contains 370 residential and industrial clients electricity usage from 2011 to 2014 with 15-min resolution. As some of the data does not start at the beginning, we collect the data from 2012-01-01 00:15:00 and delete the locations that contain more than 20 missing data. The remaining missing data (mostly because of the winter time to daylight saving time switch) is interpolated linearly. The load data is then interpolated with 3-min resolution which is consistent with the real-time control period in the grid. The final data size is 526080×232 accounting for load profiles for 232 consumers of 1096 days (three years). We then remove the outliers that are outside 7σ against the mean value. For 33-bus and 141-bus networks, the 232 load profiles are randomly assigned to each bus. For 322-bus network, repeated load profiles are allowed. In practice, Gaussian noises are added to load active and reactive powers.

PV Profiles. Ten cities/regions/provinces in Belgium, Netherlands, and Luxembourg are considered to represent the distinct zonal solar radiation levels, including Antwerp, Brussels, Flemish-Brabant (a province of Belgium), Hainaut (a province of Belgium), Liege, Limburg (a province of Netherland), Luxembourg, Namur, Walloon-Brabant (a province of Belgium), and West-Flanders (a province of Belgium). The PV data is collected from Elia group,¹⁰ a Belgium’s power network operator. The PV data is also interpolated with 3-min resolution resulting in 526080×10 data in total. For 33-bus (with 4 regions) and 141-bus (with 9 regions) networks, PV profiles are randomly assigned to each region. For 322-bus (with 22 regions) system, different regions can have the same PV profiles. Note that the

⁹<https://archive.ics.uci.edu/ml/datasets/ElectricityLoadDiagrams20112014>.

¹⁰<https://www.elia.be/en/grid-data/power-generation/solar-pv-power-generation-data>.

PVs in the same control region share the same PV profiles as they are geometrically contiguous. In real-time, we also add Gaussian noise to the PV active power.

We summarise the load and PV profiles of different scales in Figure 13-19 below.

Figure 13 illustrates the total PV active power generation and active load consumption in 33-bus network. Figure 14 illustrates four distinct PV buses in 33-bus network of January and July. Note that bus-13 and bus-18 are in the same region, so they have the same PV profiles.

Figure 15 illustrates the total PV active power generation and active load consumption in 141-bus network. Figure 16 illustrates four distinct PV buses in 141-bus network of January and July. Note that bus-36 and bus-111 are in the same region, so they have the same PV profiles.

Figure 17 illustrates the total PV active power generation and active load consumption in 322-bus network. Figure 18 illustrates four distinct PV buses in 322-bus network of January and July.

Figure 19 illustrates the power factors (PFs) of the three systems under test. Higher power factors (> 0.9) usually represents the residential consumers while low power factors (< 0.5) can represent the industrial consumers.

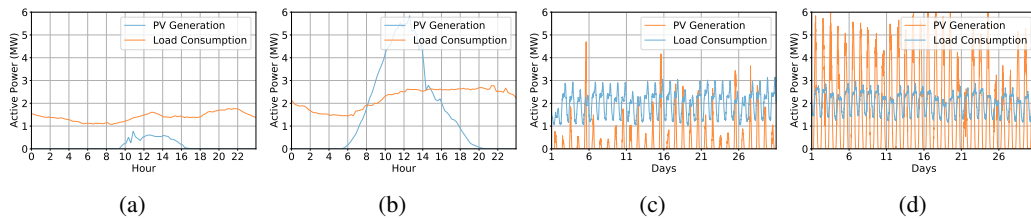


Figure 13: Total power of 33-bus network: (a): a winter day, (b): a summer day, (c): a winter month (January), (d): a summer month (July)

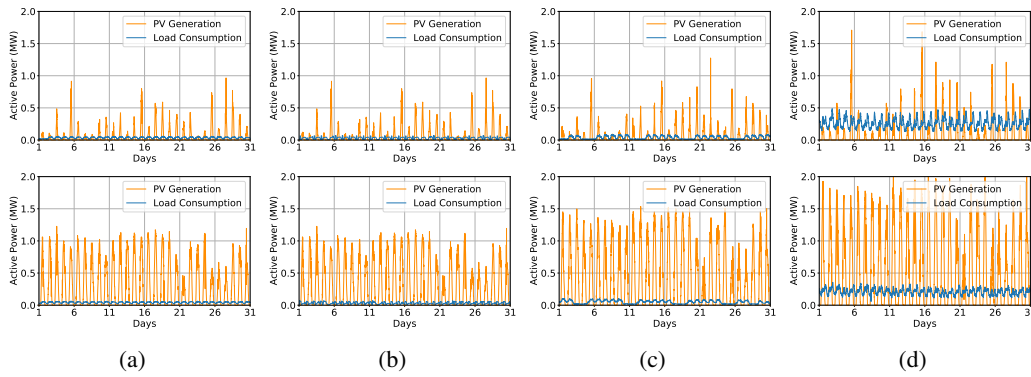


Figure 14: Daily power of 33-bus network: active PV power generation and active load consumption for different buses in 33-bus network. (a): bus-13, (b): bus-18, (c): bus-22 (d): bus-25. The first row: power in a winter month (January), second row: power in a summer month (July).

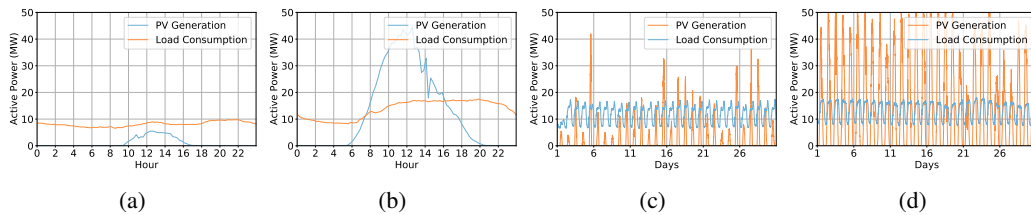


Figure 15: Total power of 141-bus network: (a): a winter day, (b): a summer day, (c): a winter month (January), (d): a summer month (July)

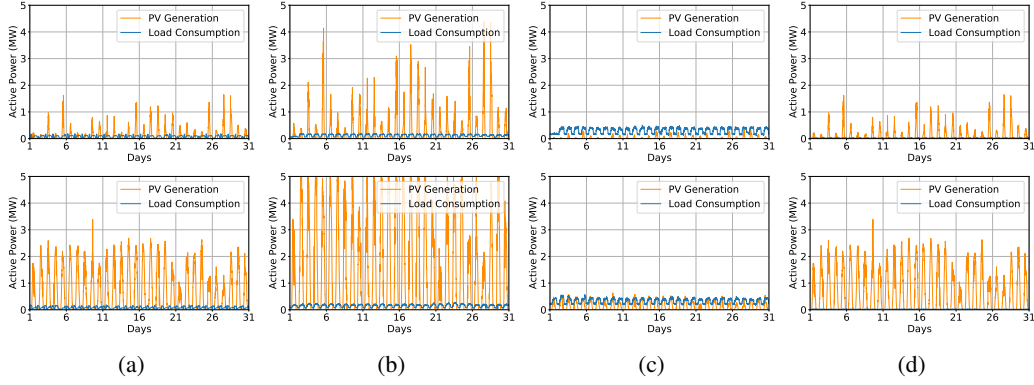


Figure 16: Daily power of 141-bus network: active PV power generation and active load consumption for different buses in 141-bus network. (a): bus-36, (b): bus-77, (c): bus-100 (d): bus-111. The first row: power in winter month (January), second row: power in summer month (July).

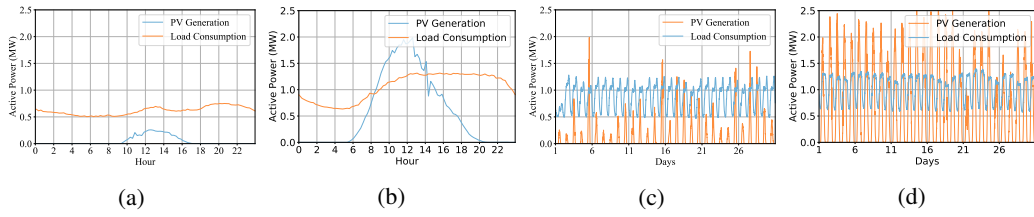


Figure 17: Total power of 322-bus network: (a): a winter day, (b): a summer day, (c): a winter month (January), (d): a summer month (July)

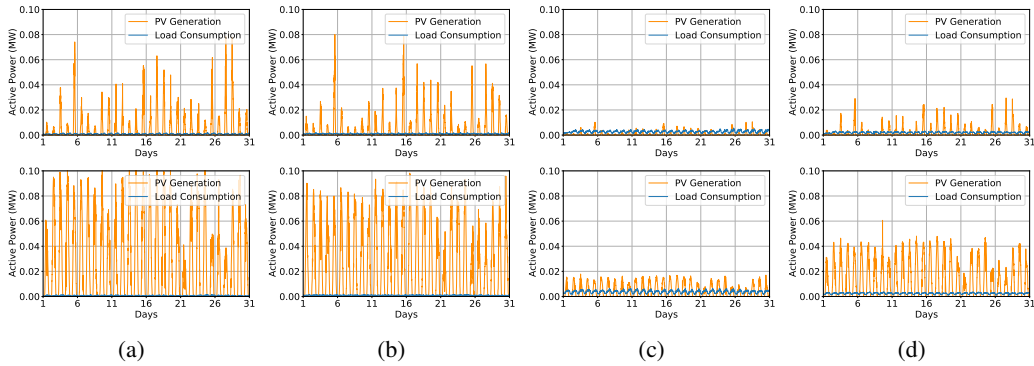


Figure 18: Daily power of 322-bus network: active PV power generation and active load consumption for different buses in 322-bus network. (a): bus-54, (b): bus-147, (c): bus-297 (d): bus-322. The first row: power in winter month (January), second row: power in summer month (July).

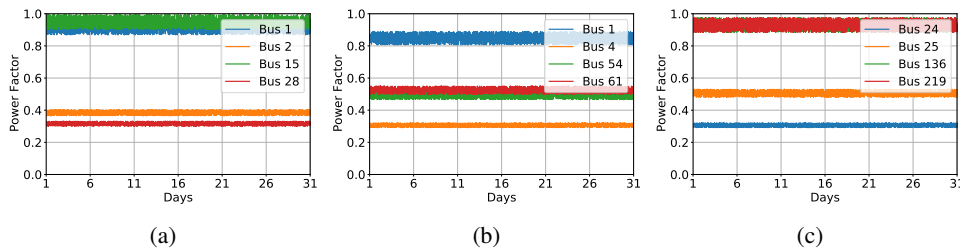


Figure 19: Power factors of four buses in (a): 33-bus, (b): 141-bus, and (c): 322-bus networks

E Extra Experimental Results

E.1 Extra Results during Training

In addition to the control rate (CR) and power loss (PL) introduced in the main part of paper, we also introduce 2 extra metrics to evaluate the performances of algorithms during training.

- *Voltage out of control ratio (VR)*: It calculates the average of the ratio of voltage outside the safety range (i.e. 0.95-1.05 *p.u.*) per time step during an episode.
- *Q loss (QL)*: It calculates the average of the mean reactive power generations by agents per time step during an episode.

Similar to the results before, all performances are measured by the median metrics of 5 random seeds and each test is conducted by 10 randomly selected episodes.

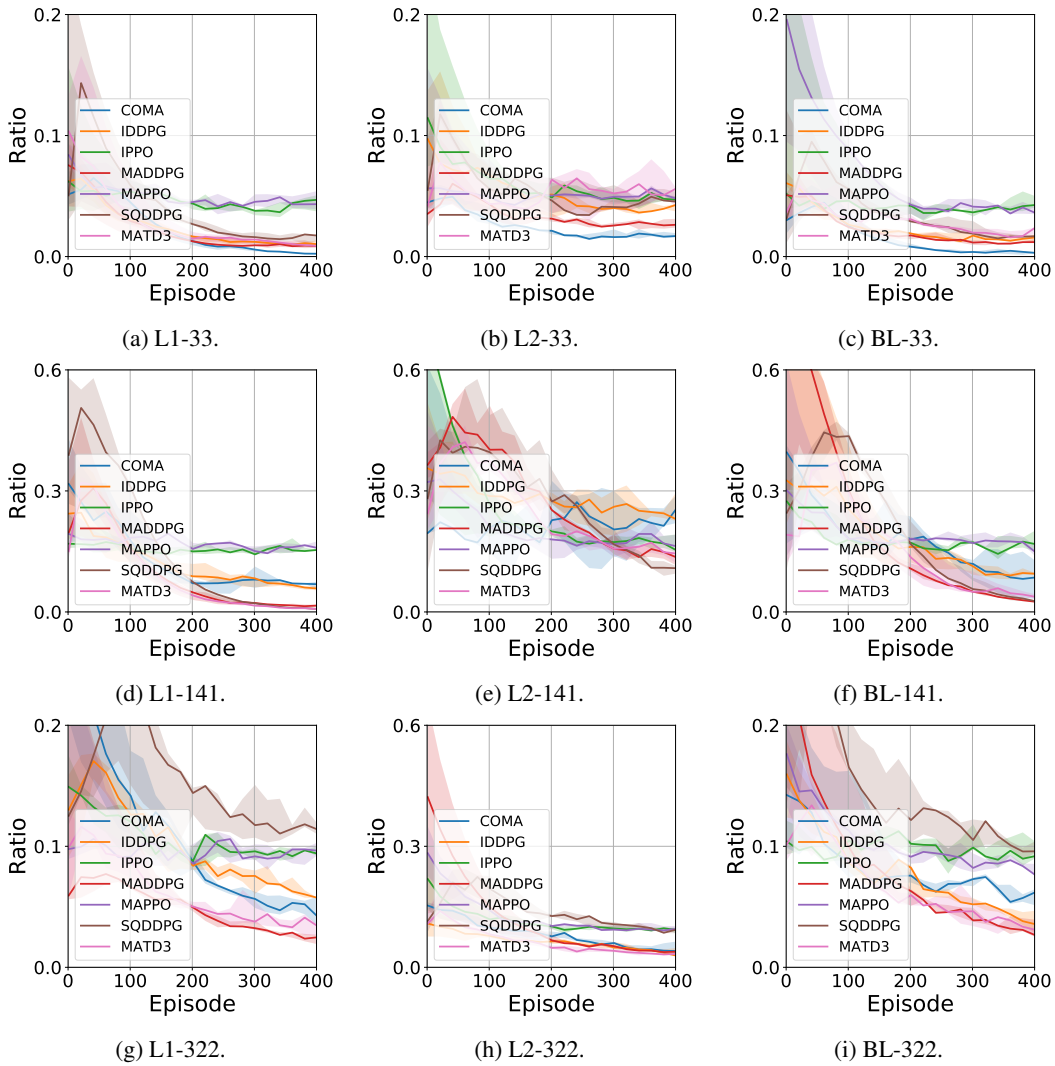


Figure 20: Voltage out of control ratio of algorithms with different reward functions consisting of distinct voltage barrier functions. The sub-caption indicates barrier-scenario and BL is the contraction of Bowl.

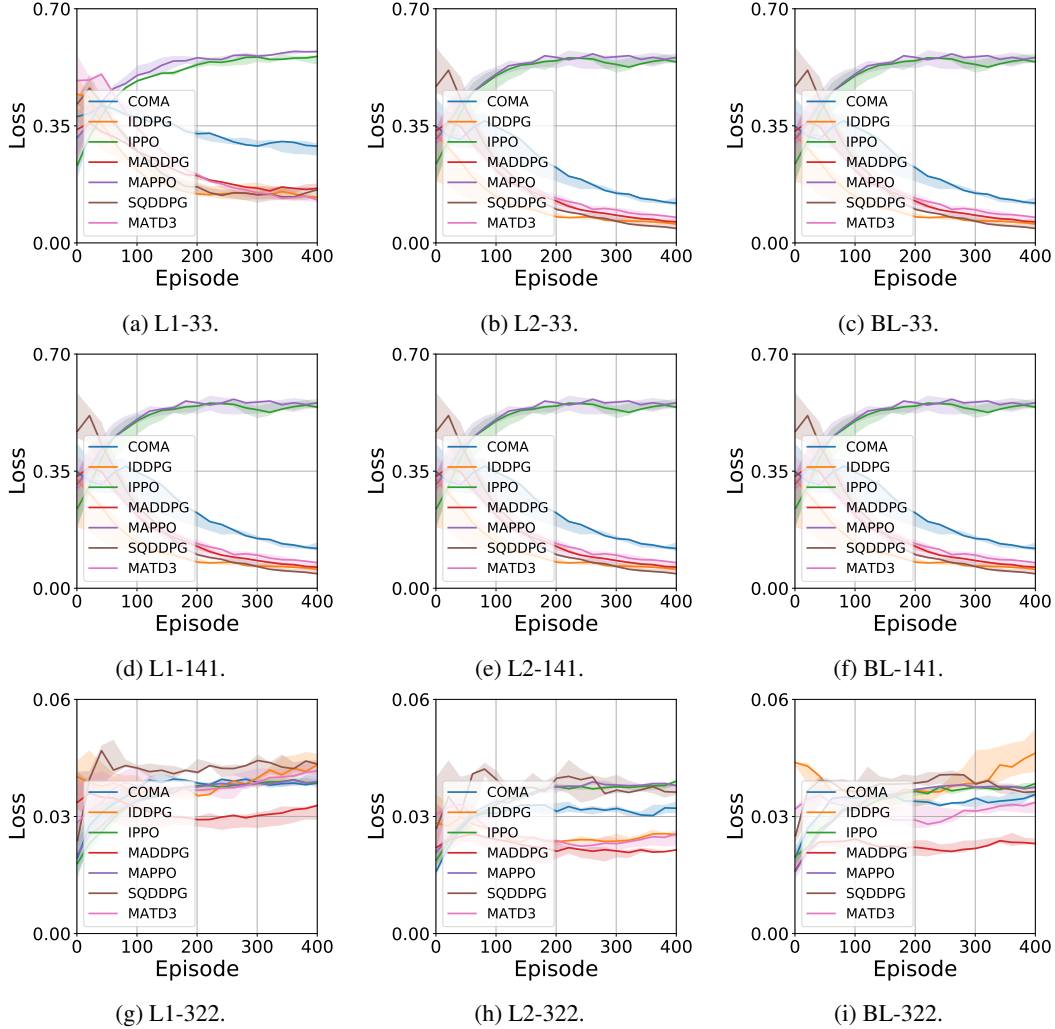


Figure 21: Q (reactive power) losses of algorithms with different reward functions consisting of distinct voltage barrier functions. The sub-caption indicates barrier-scenario and BL is the contraction of Bowl.

E.2 Extra Results for Case Studies

In this section, we show more results on the case studies for the comparison between MARL and the traditional control methods (i.e. OPF and droop control). For 141-bus network, MATD3 trained by Bowl-shape voltage barrier function acts as the candidate for MARL. For 322-bus network, MADDPG trained by L2-shape voltage barrier function acts as the candidate for MARL.

One Bus in 141-Bus Network. Figure 22 shows the results for a typical bus in the 141-bus network. In summer, all methods can control the voltage within the safety range in most of time, except that MARL fails to control the voltage from 20:00 to 22:00. Nonetheless, the power loss of MARL is lower than the droop control. In winter, all methods can control the voltage within the safety range, however, MARL behaves exclusively on generating the reactive power, i.e. generating more reactive power, while the power loss of MARL is still lower than that of the droop control.

One Bus in 322-Bus Network. Figure 23 shows the results for a typical bus in the 322-bus network. In summer, only droop control can control the voltage within the safety range. MARL and OPF cannot control the voltage within the safety range from 10:00 to 14:00 when the PV active power is extremely high. The bad performance of OPF is possibly due to the reason that the 322-bus network is so large and complicated that it may suffer the computational catastrophe w.r.t. the inverse of the

topological matrix. In winter, all methods can control the voltage within the safety range, though the voltage at this time is originally within the safety range without no control. It is so strange that MARL decrease the voltage so that it is near the lower bound of the safety range. Apparently, the strategy of MARL for this case is suboptimal. The additional penetration of reactive power by MARL induces the excessive power loss. The intrinsic reason of this phenomenon deserves to be investigated in the future work.

Analysis for All Buses. To give the whole picture of active voltage control for the days we selected for demonstrations above, we show the status of all buses in Figure 24 for the 33-bus network, Figure 25 for the 141-bus network and Figure 26 for the 322-bus network. In winter, all methods can control the voltages of all buses within the safety range whatever the scenario is. We just focus on the results for summer in the following discussion. For the 33-bus network and the 141-bus network, it is obvious that the traditional control methods can control the voltage within the safety range, while MARL loses control on some buses from 18:00 to 24:00. This implies that MARL may tend to learn solving the situations of high PV penetrations. The possible reason could be that the situations of high penetrations appear more frequently, which leads to a known problem existing in MARL called relative overgeneralisation [52]. For the 322-bus network, the performance of droop control is far better than OPF and MARL. The reason for the failure of OPF is the computational burden as we stated before. It is worth noting that droop control relies on a high-bandwidth inner loop in inverter controller so the effective control rate is much higher than the sample rate [61].

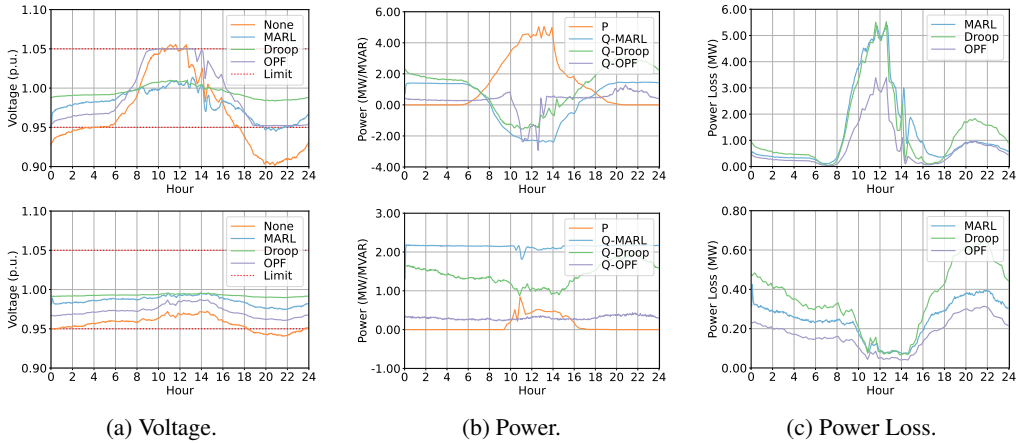


Figure 22: Compare MARL with traditional control methods on a typical bus during a day for the 141-bus network. 1st row: results for summer. 2nd row: results for winter. None and limit in (a) represent the voltage with no control and the safety range respectively. P and Q in (b) indicate the PV active power and the reactive power by various methods.

E.3 Extra Results during Testing

To show the results more convincingly, we also report the mean test results on the final models of MARL after training. The tests on each algorithm are repeated with 10 randomly selected initial states. Noticeably, we report both mean and standard deviation to exhibit the randomness of 10 tests for the metrics of continuous values. Since the metrics of ratio does not satisfy the hypothesis of normality, we just report the the mean of 10 tests for appropriateness. Additionally, we also report the results of the traditional control methods with 100 randomly selected episodes.

We now introduce the metrics used in the Table 3-5.

- *% V. Out of Control*: The average of the ratio of the voltages out of control per time step during each episode.
- *% V. below $0.95v_{ref}$* : The average ratio of the voltages below $0.95v_{ref}$ per time step during each episode.
- *% V. above $1.05v_{ref}$* : The average ratio of the voltages above $1.05v_{ref}$ per time step during each episode.

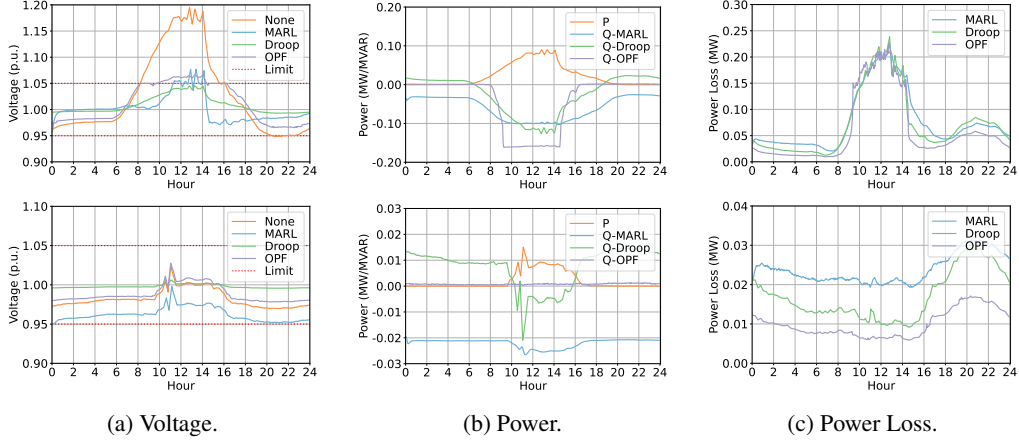


Figure 23: Compare MARL with traditional control methods on a typical bus during a day for the 322-bus network. 1st row: results for summer. 2nd row: results for winter. None and limit in (a) represent the voltage with no control and the safety range respectively. P and Q in (b) indicate the PV active power and the reactive power by various methods.

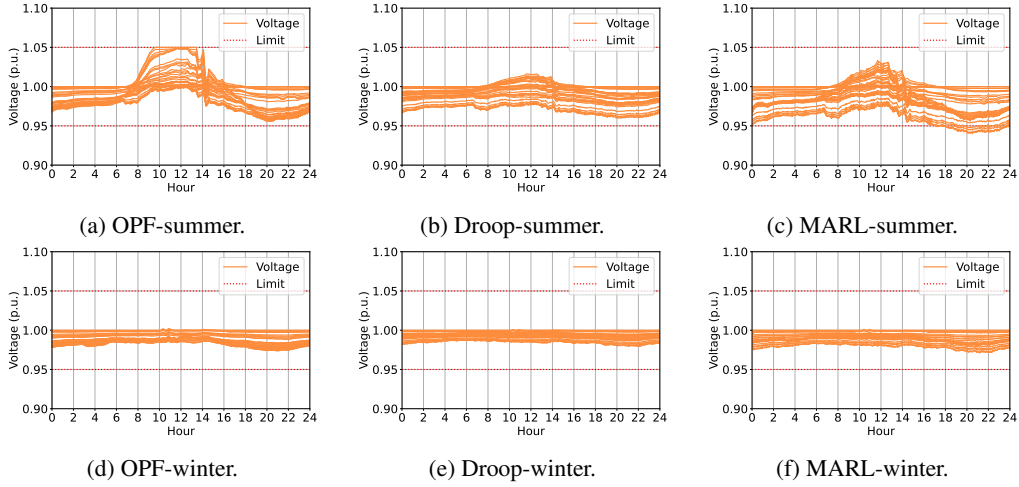


Figure 24: The status of all buses for a day on 33-bus network. The green lines are the variation of the voltage of buses and red dashed line is the safety boundary. Each caption above indicates method-season.

- *% CR*: The ratio of time steps where all buses' voltages being under control during each episode.
- *V. Dev.*: The average voltage deviations (away from the v_{ref}) during each episode.
- *Max V. Drop Dev.*: The average of the maximum deviation of voltage drop (i.e. below $0.95v_{ref}$) per time step during each episode.
- *Max V. Rise Dev.*: The average of the maximum deviation of voltage rise (i.e. above $1.05v_{ref}$) per time step during each episode.
- *PL*: The average of the total power loss over all buses per time step during each episode.

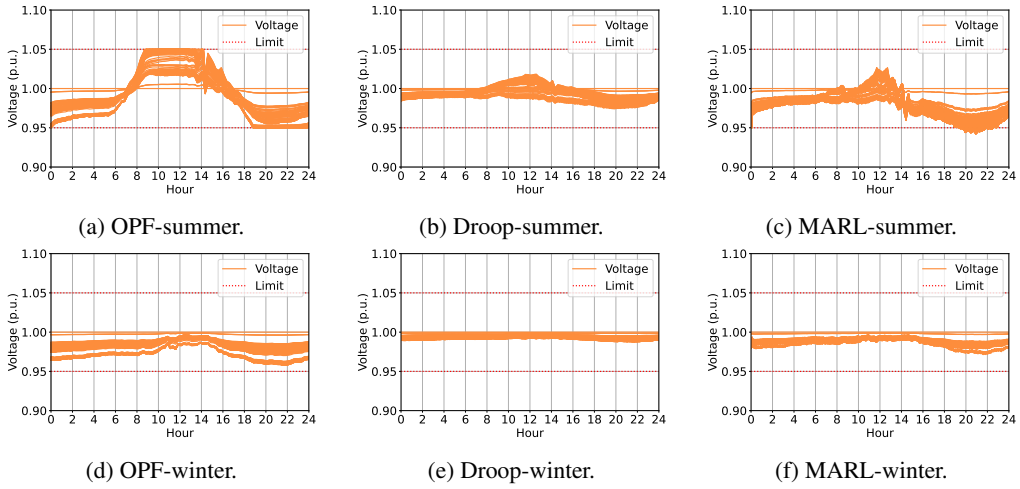


Figure 25: The status of all buses for a day on 141-bus network. The green lines are the variation of the voltage of buses and red dashed line is the safety boundary. Each caption above indicates method-season.

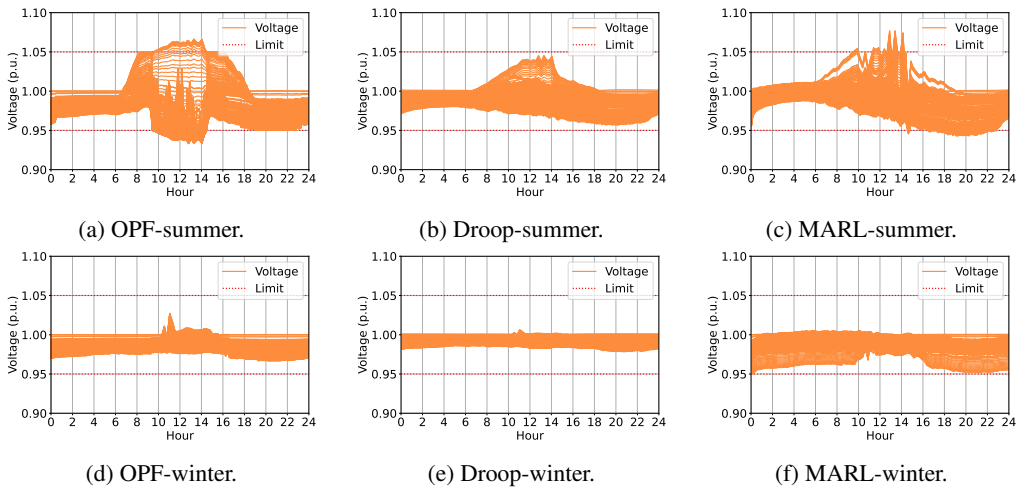


Figure 26: The status of all buses for a day on 322-bus network. The green lines are the variation of the voltage of buses and red dashed line is the safety boundary. Each caption above indicates method-season.

Table 3: The mean test results on the 33-bus network with 10 randomly selected episodes for MARL and 100 random selected episodes for the traditional control methods. The results are recorded with mean (\pm std.).

METHOD	% V. OUT OF CONTROL	% V. BELOW	% V. ABOVE	% CR	V. DEV.	MAX V. DROP DEV.	MAX V. RISE DEV.	PL
NO CONTROL	6.3	5.1	1.2	70.6	0.021 \pm 0.005	0.036 \pm 0.011	0.010 \pm 0.015	0.069 \pm 0.036
DRPOOP CONTROL	0.0	0.0	0.0	100.0	0.011 \pm 0.002	0.025 \pm 0.006	0.003 \pm 0.004	0.082 \pm 0.064
OPF	0.0	0.0	0.0	100.0	0.014 \pm 0.003	0.020 \pm 0.009	0.011 \pm 0.013	0.056 \pm 0.046
IDDPG-L1	1.1	0.7	0.4	90.3	0.014 \pm 0.002	0.000 \pm 0.000	0.001 \pm 0.000	0.066 \pm 0.007
MADDPG-L1	0.9	0.4	0.5	92.0	0.013 \pm 0.000	0.000 \pm 0.000	0.001 \pm 0.000	0.071 \pm 0.004
COMA-L1	0.2	0.0	0.2	97.0	0.011 \pm 0.000	0.000 \pm 0.000	0.000 \pm 0.000	0.105 \pm 0.002
IPPO-L1	4.5	0.0	4.5	68.1	0.015 \pm 0.001	0.000 \pm 0.000	0.008 \pm 0.002	0.148 \pm 0.010
MAPPO-L1	4.5	0.0	4.5	68.2	0.015 \pm 0.001	0.008 \pm 0.002	0.008 \pm 0.002	0.154 \pm 0.005
MATD3-L1	1.0	0.8	0.2	91.6	0.015 \pm 0.001	0.000 \pm 0.000	0.000 \pm 0.000	0.064 \pm 0.004
SQDDPG-L1	1.5	0.8	0.3	87.2	0.015 \pm 0.001	0.000 \pm 0.000	0.001 \pm 0.000	0.068 \pm 0.005
IDDPG-L2	4.4	3.5	0.9	75.4	0.020 \pm 0.001	0.001 \pm 0.000	0.001 \pm 0.001	0.067 \pm 0.005
MADDPG-L2	2.8	2.0	0.8	79.7	0.018 \pm 0.000	0.001 \pm 0.000	0.001 \pm 0.000	0.063 \pm 0.004
COMA-L2	1.7	0.9	0.8	85.8	0.015 \pm 0.001	0.000 \pm 0.000	0.001 \pm 0.000	0.068 \pm 0.004
IPPO-L2	4.5	0.1	4.5	72.0	0.015 \pm 0.001	0.000 \pm 0.000	0.009 \pm 0.001	0.142 \pm 0.008
MAPPO-L2	4.7	0.0	4.7	70.9	0.015 \pm 0.000	0.000 \pm 0.000	0.010 \pm 0.001	0.139 \pm 0.005
MATD3-L2	5.4	4.9	0.5	75.0	0.021 \pm 0.001	0.002 \pm 0.001	0.001 \pm 0.000	0.074 \pm 0.004
SQDDPG-L2	4.9	3.9	1.1	74.0	0.021 \pm 0.001	0.001 \pm 0.000	0.002 \pm 0.001	0.071 \pm 0.003
IDDPG-BL	1.5	1.2	0.3	87.0	0.015 \pm 0.000	0.012 \pm 0.003	0.003 \pm 0.003	0.069 \pm 0.007
MADDPG-BL	1.2	1.0	0.2	89.0	0.015 \pm 0.001	0.010 \pm 0.003	0.002 \pm 0.001	0.073 \pm 0.004
COMA-BL	0.3	0.2	0.2	96.5	0.011 \pm 0.000	0.002 \pm 0.001	0.002 \pm 0.001	0.106 \pm 0.005
IPPO-BL	4.6	0.1	4.5	65.4	0.015 \pm 0.001	0.001 \pm 0.001	0.045 \pm 0.008	0.154 \pm 0.013
MAPPO-BL	3.8	0.1	3.7	70.6	0.014 \pm 0.001	0.001 \pm 0.001	0.037 \pm 0.006	0.150 \pm 0.008
MATD3-BL	2.2	2.0	0.2	84.0	0.019 \pm 0.001	0.020 \pm 0.002	0.002 \pm 0.001	0.077 \pm 0.009
SQDDPG-BL	1.8	1.1	0.7	85.4	0.016 \pm 0.001	0.011 \pm 0.005	0.007 \pm 0.002	0.072 \pm 0.007

Table 4: The mean test results on the 141-bus network with 10 randomly selected episodes for MARL and 100 random selected episodes for the traditional control methods. The results are recorded with mean (\pm std.).

METHOD	% V. OUT OF CONTROL	% V. BELOW	% V. ABOVE	% CR	V. DEV.	MAX V. DROP DEV.	MAX V. RISE DEV.	PL
NO CONTROL	32.3	23.8	8.6	37.9	0.042 \pm 0.008	0.046 \pm 0.021	0.016 \pm 0.022	0.956 \pm 0.610
DRPOOP CONTROL	0.0	0.0	0.0	100.0	0.009 \pm 0.002	0.014 \pm 0.003	0.003 \pm 0.004	1.519 \pm 1.335
OPF	0.0	0.0	0.0	100.0	0.021 \pm 0.006	0.020 \pm 0.008	0.011 \pm 0.012	0.819 \pm 0.922
IDDPG-L1	9.7	7.7	2.0	71.9	0.026 \pm 0.002	0.003 \pm 0.002	0.001 \pm 0.000	1.167 \pm 0.137
MADDPG-L1	2.4	1.1	1.3	92.3	0.016 \pm 0.002	0.000 \pm 0.000	0.001 \pm 0.000	1.525 \pm 0.137
COMA-L1	8.9	7.2	1.6	73.9	0.023 \pm 0.007	0.004 \pm 0.004	0.001 \pm 0.001	1.639 \pm 0.216
IPPO-L1	13.8	0.0	13.8	77.3	0.026 \pm 0.002	0.000 \pm 0.000	0.011 \pm 0.002	1.380 \pm 0.061
MAPPO-L1	16.0	0.1	15.9	74.6	0.028 \pm 0.002	0.000 \pm 0.000	0.013 \pm 0.002	1.465 \pm 0.069
MATD3-L1	2.3	0.4	1.9	94.1	0.015 \pm 0.001	0.000 \pm 0.000	0.001 \pm 0.001	1.608 \pm 0.107
SQDDPG-L1	1.8	0.7	1.0	96.0	0.015 \pm 0.001	0.001 \pm 0.000	0.001 \pm 0.000	1.757 \pm 0.064
IDDPG-L2	26.0	20.1	5.9	49.3	0.038 \pm 0.003	0.008 \pm 0.002	0.004 \pm 0.001	0.966 \pm 0.085
MADDPG-L2	12.6	9.3	3.3	68.9	0.028 \pm 0.002	0.003 \pm 0.001	0.002 \pm 0.000	1.007 \pm 0.098
COMA-L2	26.6	16.1	10.5	41.4	0.038 \pm 0.005	0.016 \pm 0.011	0.012 \pm 0.005	1.989 \pm 0.369
IPPO-L2	16.7	0.2	16.5	72.9	0.028 \pm 0.003	0.000 \pm 0.000	0.013 \pm 0.003	1.418 \pm 0.129
MAPPO-L2	17.1	0.1	17.0	72.6	0.029 \pm 0.002	0.000 \pm 0.000	0.014 \pm 0.002	1.472 \pm 0.043
MATD3-L2	14.6	11.3	3.3	63.9	0.030 \pm 0.003	0.004 \pm 0.001	0.002 \pm 0.001	0.954 \pm 0.063
SQDDPG-L2	14.3	10.2	4.2	67.1	0.029 \pm 0.007	0.006 \pm 0.006	0.003 \pm 0.002	1.350 \pm 0.257
IDDPG-BL	8.8	7.2	1.6	74.3	0.025 \pm 0.003	0.003 \pm 0.001	0.001 \pm 0.000	1.136 \pm 0.110
MADDPG-BL	2.5	1.6	0.9	91.6	0.020 \pm 0.001	0.001 \pm 0.000	0.001 \pm 0.000	1.350 \pm 0.088
COMA-BL	9.3	6.8	2.5	72.0	0.024 \pm 0.005	0.004 \pm 0.004	0.002 \pm 0.002	1.954 \pm 0.413
IPPO-BL	17.5	0.1	17.4	72.2	0.029 \pm 0.002	0.000 \pm 0.000	0.014 \pm 0.003	1.450 \pm 0.052
MAPPO-BL	15.8	0.1	15.7	75.0	0.028 \pm 0.003	0.000 \pm 0.000	0.013 \pm 0.003	1.500 \pm 0.133
MATD3-BL	5.8	4.3	1.4	81.3	0.021 \pm 0.005	0.002 \pm 0.003	0.001 \pm 0.000	1.313 \pm 0.086
SQDDPG-BL	2.9	1.5	1.5	92.1	0.016 \pm 0.001	0.001 \pm 0.000	0.001 \pm 0.000	1.720 \pm 0.235

Table 5: The mean test results on the 322-bus network with 10 randomly selected episodes for MARL and 100 random selected episodes for the traditional control methods. The results are recorded with mean (\pm std.).

METHOD	% V. OUT OF CONTROL	% V. BELOW	% V. ABOVE	% CR	V. DEV.	MAX V. DROP DEV.	MAX V. RISE DEV.	PL
No CONTROL	18.2	15.6	2.5	32.1	0.032 \pm 0.006	0.052 \pm 0.013	0.028 \pm 0.035	0.038 \pm 0.017
DROOP CONTROL	0.0	0.0	0.0	99.4	0.011 \pm 0.002	0.027 \pm 0.005	0.008 \pm 0.008	0.061 \pm 0.043
OPF	5.0	4.6	0.3	86.8	0.015 \pm 0.008	0.026 \pm 0.010	0.018 \pm 0.014	0.057 \pm 0.036
IDDPG-L1	6.1	1.5	4.6	36.7	0.018 \pm 0.002	0.007 \pm 0.004	0.015 \pm 0.006	0.109 \pm 0.013
MADDPG-L1	2.3	0.1	2.2	77.7	0.013 \pm 0.001	0.000 \pm 0.000	0.009 \pm 0.002	0.070 \pm 0.007
COMA-L1	4.7	0.2	4.5	56.6	0.017 \pm 0.002	0.000 \pm 0.000	0.016 \pm 0.004	0.091 \pm 0.008
IPPO-L1	9.3	0.1	9.2	39.1	0.024 \pm 0.001	0.000 \pm 0.000	0.037 \pm 0.005	0.103 \pm 0.003
MAPPO-L1	9.8	0.1	9.7	40.0	0.024 \pm 0.001	0.000 \pm 0.000	0.039 \pm 0.004	0.102 \pm 0.004
MATD3-L1	3.2	1.3	1.9	64.8	0.015 \pm 0.001	0.004 \pm 0.003	0.008 \pm 0.002	0.078 \pm 0.007
SQDDPG-L1	11.7	0.3	11.4	29.6	0.026 \pm 0.001	0.001 \pm 0.001	0.042 \pm 0.006	0.117 \pm 0.013
IDDPG-L2	3.6	0.9	2.7	65.9	0.016 \pm 0.001	0.001 \pm 0.001	0.011 \pm 0.004	0.070 \pm 0.010
MADDPG-L2	3.8	0.6	3.2	67.3	0.016 \pm 0.001	0.001 \pm 0.000	0.015 \pm 0.003	0.053 \pm 0.004
COMA-L2	4.9	0.2	4.7	51.1	0.017 \pm 0.002	0.000 \pm 0.000	0.016 \pm 0.006	0.081 \pm 0.007
IPPO-L2	9.1	0.1	9.0	39.7	0.024 \pm 0.001	0.000 \pm 0.000	0.036 \pm 0.004	0.103 \pm 0.004
MAPPO-L2	10.0	0.1	9.9	40.5	0.024 \pm 0.002	0.000 \pm 0.000	0.040 \pm 0.006	0.100 \pm 0.007
MATD3-L2	3.1	0.5	2.6	71.1	0.015 \pm 0.001	0.001 \pm 0.000	0.012 \pm 0.003	0.058 \pm 0.007
SQDDPG-L2	9.1	0.3	8.8	44.0	0.023 \pm 0.001	0.000 \pm 0.000	0.036 \pm 0.004	0.097 \pm 0.007
IDDPG-BL	4.7	1.1	3.6	40.9	0.017 \pm 0.003	0.005 \pm 0.005	0.012 \pm 0.004	0.128 \pm 0.024
MADDPG-BL	3.2	0.9	2.3	67.7	0.016 \pm 0.001	0.001 \pm 0.001	0.011 \pm 0.005	0.065 \pm 0.008
COMA-BL	5.7	0.2	5.5	43.2	0.017 \pm 0.001	0.001 \pm 0.001	0.018 \pm 0.004	0.098 \pm 0.010
IPPO-BL	9.3	0.1	9.2	41.0	0.024 \pm 0.001	0.000 \pm 0.000	0.037 \pm 0.005	0.101 \pm 0.003
MAPPO-BL	8.2	0.1	8.1	44.6	0.022 \pm 0.001	0.000 \pm 0.000	0.032 \pm 0.004	0.097 \pm 0.003
MATD3-BL	2.8	0.8	2.0	68.1	0.016 \pm 0.001	0.001 \pm 0.001	0.010 \pm 0.003	0.074 \pm 0.006
SQDDPG-BL	9.7	0.2	9.5	40.6	0.024 \pm 0.001	0.000 \pm 0.000	0.039 \pm 0.003	0.100 \pm 0.012